BLOOD FLOW EFFECTS ON HEART DEVELOPMENT AND A MINIMALLY INVASIVE TECHNIQUE FOR *IN VIVO* FLOW ALTERATIONS

Thesis by

Gabriel Alejandro Acevedo Bolton

In Partial Fulfillment
of the Requirements for the Degree of
Doctor of Philosophy

California Institute of Technology

Pasadena, California

2005

(Defended December 15, 2004)

Acknowledgements

I would like to thank my advisor, Professor Mory Gharib for his guidance, patience, and contagious enthusiasm throughout my time at Caltech. His fascination with the world around us, including things that many of us take for granted, continues to inspire me. I also would like to express my thanks to him for opening up his home and family to me.

I would also like to thank Professor Jay Hove, who served on my committee, for his immensely important ideas and comments during the process of completing this thesis. I also would like to thank the other members of my committee: Professors Scott Fraser and Michael Dickinson.

I would not have been able to complete the work I did without the help of others at Caltech. In particular, I would like to thank Dr. Mladen Barbic for constructing and providing the magnets and for his patience in repairing them after my rough handling, the members of Professor Fraser's Biological Imaging Center for teaching me about imaging and zebrafish and for making me feel at home, and last but not least, the Gharib group for teaching me about DPIV and everything fluids related.

I would also like to thank those people who made life at Caltech more fun. Thanks to my office mate and comrade, David Jeon, for his company and for sharing my love of Peruvian magic sauce, fish tacos, and espresso. Thanks to

my first friends at Caltech, Tait Pottebaum and Matt Fago, for their continuing friendship and for helping me stick out that first year of Aero. Thanks to Kathleen Hamilton and Martha Salcedo, who went way beyond the call of duty for me, and of course for all of the enjoyable chats and gossip that we shared.

Finally, thanks to Hannah and to my family. Their love and support have kept me afloat even during the most difficult times.

This thesis is dedicated to my wife and the love of my life, Hannah. Her love, faith in my abilities, and sense of humor throughout the process (and our entire time together) have supported me more than she knows.

Abstract

A series of experiments were conducted on zebrafish (*Danio rerio*) in order to gain a better understanding of how blood flow and blood flow related forces, such as shear stress, affect vertebrate heart development. Zebrafish were used as a model due to their external fertilization and optical accessibility to the heart and vasculature. The flow field inside the 4.5 day post fertilization (dpf) embryo was analyzed using a combination of manual particle tracking and digital particle image velocimetry (DPIV) software. Our results present the first case of intracardiac microscale DPIV. Additionally, a minimally invasive and reversible technique of delivering and localizing magnetic microspheres inside the vasculature of the embryo was developed. The results of blocked flow induced with this method were compared with previous experiments and controls.

The results of the flow field analysis showed the existence of an extremely dynamic flow environment containing jets with a velocity of 5 mm/s and regions of vorticity in a low Reynolds number environment. Calculations of the flow at the 4.5 dpf A-V resulted in wall shear stress levels of 70 dynes/cm^2, levels much higher than needed for endothelial cell response.

We also showed that injected magnetic microspheres can be delivered and localized within the embryonic vasculature to reversibly block blood flow in the dorsal artery and at the inflow to the heart. Blocked blood flow of 12 hours and longer resulted in lower blood velocity and a less developed heart, exhibiting

edema, regurgitance, decreased contractile function, and delayed development. These findings are consistent with previous studies showing that blood flow is a necessary factor for heart development. Furthermore an unexpected result was observed. Exposure to a localized magnetic field eventually caused the absorption of magnetic microspheres into the surrounding tissue. It is theorized that this could be utilized in future studies modeling the effects of reduced cardiac contractility.

Table of Contents

List of figures

List of Tables

Chapter 1: Introduction

1.1 Introduction

The development of the vertebrate heart is of great interest to the fields of science and medicine. The heart is the first organ to form and is necessary for the distribution of blood throughout the developing embryo. Furthermore, errors in cardiogenesis are the leading form of congenital birth defects (Olson *et al.,* 1996). Many conditions must be met to ensure proper heart development. Over the last century experiments have shown that both genetic programming and epigenetic factors, such as blood flow induced forces, can affect both normal and patho-physiological cardiac development. Nevertheless, how epigenetic factors and genetic programming interact remains poorly understood.

A better understanding of the subtle interplay between these processes, and their role in controlling heart development, offers the potential to begin to uncover the etiology of congenital heart diseases, many of which are believed to have their origins during embryonic development (O'Brien, 1999).

The difficulty of imaging blood flow *in vivo* has in turn made it difficult to ascertain the role of epigenetic factors, such as blood flow and pressure, in controlling heart development. Recent technological advances (i.e., high-speed confocal microscopy, high-speed CCD cameras, and flow visualization software) now allow us to make these kinds of quantitative flow measurements. Simple observation of the blood flow is not sufficient to understand the role it plays in

heart development. In order to demonstrate whether or not the fluid dynamic forces produced by blood flowing within a closed-circuit vascular system actually influence cardiac morphogenesis, we must devise a technique for: i) quantitatively measuring and ii) experimentally altering the flow environment *in vivo.* With the results of this technique we wish to correlate subsequent changes in blood flow patterns to developmental morphology. It is the purpose of this dissertation to develop a minimally invasive method of creating localized flow disturbances in order to better understand the role of blood flow in heart development.

1.2 Background

1.2.1 *Zebrafish Heart Formation*

The zebrafish (*Danio rerio*) has become an important biological model since its introduction to science nearly two decades ago (Streisinger *et al*., 1981). External fertilization, rapid development, ease of handling, and profound optical accessibility have led to its widespread use in biological research (Hove, 2004). Pelster and Burggren (1996), through a series of experiments that blocked hemoglobin-facilitated oxygen transport, showed that due to their small size, zebrafish are able to obtain oxygen and nutrients through diffusion alone for the first 5 to 7 days post fertilization (dpf). The ability to survive without a functioning heart or circulation has made the zebrafish an indispensable model for vertebrate heart development. Perhaps the most important aspect of zebrafish physiology for biological studies is their optical transparency. Zebrafish are naturally

transparent until approximately 32 hours post fertilization (hpf). Subsequent melanin formation can be prevented for several days by exposure to 1-phenyl 2-thio-urea (PTU) between 18-24 hpf (Karlsson *et al*., 2001). This optical accessibility coupled with external fertilization gives researchers unparalleled access to development as compared to mammalian and avian models. Zebrafish hold relevance to human heart development since, as vertebrates, the early developmental stages are evolutionarily conserved.

The zebrafish heart is a two-chambered organ consisting of an atrium and ventricle that begins to acquire its characteristic shape at 72 hpf, although the cardiogenetic process begins much earlier. Differentiation of zebrafish myocardial precursors begins around 16 hpf, when these cells reside within bilateral regions of rostral lateral plate mesoderm. Integration of these lateral populations into a single heart tube requires their migration toward the midline, which occurs in concert with the medial movement of the entire rostral lateral plate mesoderm. Cardiac migration appears to proceed in an organized fashion, with the medially located ventricular precursors advancing ahead of the laterally located atrial precursors (Yelon *et al*., 1999).

Once the myocardial precursors reach the midline (~18 hpf), they begin to interact and combine in a process called cardiac fusion. Initial contact occurs when the two myocardiocytes caudal to the initial junction join each other, creating a V-shape. Finally, the most rostral portions of both populations connect, creating a rostral border to a central lumen. Viewed laterally, it is

apparent that the myocardiocytes have formed a shallow cone, with its ventricular apex raised dorsally above its atrial base (Yelon *et al*., 1999).

Following cardiac fusion, the cardiac cone extends, gradually converting into a linear heart tube by 24 hpf. At about 30 hpf the linear heart tube begins to gradually bend at the boundary between the ventricle and the atrium to create an S-shaped loop with the heart tube to the right, resulting in the atrium lying to the right and slightly dorsal of the ventricle. This looping is considered the test for left-right heart asymmetry (Chen *et al*., 1997; Chin *et al*., 2000). The looping process, usually completed in about 6 hours (Stainier, 2001), is common to all vertebrates.

The heart tube begins to function as soon as it forms. Contraction begins at 22 hpf at a rate of 90 contractions per minute (Stanier *et al*., 1993) and drives circulation with regular contractions by 26 hpf (Kimmel *et al*., 1995). This flow becomes unidirectional despite lack of valves at 36 hpf, using sequential contractions (Warren and Fishman, 1998). Coinciding with the initiation of heart contraction, blood cell differentiation occurs in a region called the intermediate cell mass (ICM) that lies dorsal to the yolk tube (Thisse and Zon, 2002). While the heart is working, cardiac differentiation and morphogenesis continue, building on the foundation of the initial embryonic tube to produce the final form of the adult heart. In addition to cardiac looping, other aspects of cardiac remodeling include valve formation, thickening of the ventricular wall, and the formation of ventricular trabeculae (finger-like projections of myocardium). Recent work has

begun to investigate the molecular mechanisms responsible for these modifications that enhance cardiac function (Hu *et al*., 2000, 2001).

The heart develops two sets of valves, the atrio-ventricular (AV) and ventriculo-bulbus (V-B) valves. A-V valve formation begins with the formation of endocardial cushions at the atrioventricular boundary by 48 hpf. These cushions are later replaced by fully functional valves by 5 dpf (Hu *et al.*, 2000). Endocardial cushions are believed to be created by an epithelial–mesenchymal transformation that is stimulated by signaling between specialized endocardial and myocardial cells at the atrioventricular boundary (Eisenberg and Markwald, 1995).

1.2.2 *Genetic Factors in Heart Development*

Zebrafish have also particularly become a popular model for studying genetic aspects of vertebrate development. Zebrafish are particularly well suited for loss of heart function experiments as, unlike chicks or mice, they are not dependent on blood flow for early survival. Given the advances in DNA sequencing and genetic screening, it is not surprising that a large number of genes have been shown to play a role in heart development. Stanier *et al.* (1996) list 58 mutations, which affect the function and morphogenesis of the heart and vascular system in zebrafish. They can be grouped by effect or phenotype. Descriptions of some of the mutations affecting cardiac morphogenesis include: i) *Cloche,* which prevents the endocardium from developing; ii) *Valentine, Heart of Glass,* and *Santa* mutations, which result in an oversized and distended heart; iii)

Heart and Soul, which results in a smaller heart; iv) *Pandora*, which causes ventricle defects; v) *Miles Apart* and *Bonnie and Clyde* ,which prevent the two cardiac primordial tubes from fusing, thus developing two independently contracting linear heart tubes and; vi) the *Jekyll* mutation, which prevents valve formation in the heart.

Since Stanier's 1996 paper, many more mutations have been discovered that influence zebrafish heart development. Notably, Reiter *et al*. (1999) showed that a mutation in the GATA5 zinc finger transcription factor led to cardia bifida, or two independent linear heart tubes. Additionally, the *Hand* gene has been shown to be responsible for the morphogenesis of the ventricle (Yelon, 2000), and *silent heart* embryos lack a heartbeat (Sehnert *et al*., 2002). It is certain that with more screens and sequencing data, yet more essential genes will be found that play a critical role in heart development.

Along with specific gene knock outs, experiments show that neural crest ablation leads to cardiovascular and hemodynamic deficiencies. Experiments in which the neural crest cells in chicks were ablated resulted in outflow track abnormalities and also altered flow patterns in the developing heart tube, even before contraction began (reviewed by Creazzo, 1998).

These types of genetic and ablation studies are important because they demonstrate that there is certainly a major role for genetic programming in vertebrate heart development. These studies begin to clarify the necessary steps and sequences that genetics play in developing the heart. However, despite the knowledge that certain genes or transcription factors are needed for normal heart

development, these studies alone cannot answer the question of what controls the activation of these genes in different cases and how epigenetic variables factor in.

1.2.3 *Endothelial Cell Response to Blood Flow*

Since it has traditionally been difficult to observe the effect of blood flow on the vasculature *in vivo,* most experiments have been conducted *in vitro*. One important area of study in the field of biofluid dynamics is the effect of blood flow on vascular endothelial cells. Many of these studies have been motivated by the apparent relationship between the onset of atherosclerosis, a condition in which hard plaques build up along the arterial wall, and localized blood flow conditions. Atherosclerosis can cause hardening of the arteries, flow blockage, and in serious cases stroke. The flow-dependent nature of atherosclerosis is based on the observation that plaque formation seemed to be localized within bifurcations and bends in the arteries, regions where the blood flow is disturbed. Perhaps more revealing was the realization that in these bifurcations and bends, the plaques mostly tended to form on the outside curves, which are regions of flow separation and lower shear stress (Jou and Berger, 1998; Jou and Saloner, 1998). In an effort to better understand the link between flow and the onset of atherosclerosis, researchers focused on the response of endothelial cells to blood flow.

Endothelial cells (ECs), which line the entire vasculature in vertebrates, act as a barrier between the blood stream and the rest of the body by selectively allowing certain nutrients and cells to pass through, while keeping others out.

Additionally, they also act as force sensors and transducers. *In vitro* experiments conducted by Fry *et al.* (1965), Caro *et al.* (1969), Davies *et al.* (1989), Dewey *et al.* (1981), and others showed that ECs responded to varying levels of shear stress. Olesen (1988) found that the cells could sense levels of shear stress as low as 0.2 dyne/cm^2. Cellular response depends on both the magnitude and direction of shear stress applied to the ECs.

Endothelial cells respond differentially under conditions of low or high shear stress. Under conditions of low shear stress, defined as less than 4 dyne/cm^2, cells produce higher levels of compounds such as adhesion molecules, inflammatory mediators, and vasoconstrictors, which lead to an atherosclerotic phenotype. Conversely, at levels of shear stress greater than 15 dyne/cm^2, cells decrease production of the agents listed above and increase production of vasodilators, anti-oxidants, and growth inhibitors, protecting the cells from atherosclerosis (reviewed by Malek *et al.,* 1999). This research has led to the conclusion that to remain healthy, ECs need to be exposed to a minimum level of shear stress. If the shear stress drops below this level, or extensive retrograde flow exists, the process of atherosclerosis is facilitated (Gharib and Beizaie, 2003).

1.2.4 *Flow Alteration Studies*

The notion of flow affecting heart development is partly based on *in vitro* studies, which show that ECs, which comprise the lumen of the entire cardiovascular system, change their morphology, orientation, behavior, and transcription patterns as a result of changes in flow conditions. As the heart's

luminal surface is lined with endothelial cells, the notion of heart development also changing to flow conditions is reasonable.

However, with regard to the flow-dependent effects of heart development, studies will remain highly speculative until the intracardiac milieu in developing hearts has been quantitatively analyzed. Flow across a cultured monolayer of cells is largely one-dimensional, unlike the flow one would expect *in vivo*. Furthermore, it seems likely that a monolayer of cultured cells interacts quite differently from ECs in their natural environment (Davies *et al.*, 1995), which grow on a basal membrane and interact with the additional underlying layers. In order to truly establish the importance of blood flow on not only ECs, but also heart development, flow studies will have to be conducted in the system's natural environment, i.e., *in vivo*.

The mechanisms responsible for early heart development, and particularly for looping, have been debated since the late 1800s. At that time, most researchers could be divided into two different schools of thought. One believed that heart looping was completely intrinsic and preprogrammed (e.g., Stohr, 1924, 1925, 1927), whereas the other believed that flow was responsible for proper heart development. On the flow-dependence side, the belief was that heart tube looping was a result of asymmetric flow impinging differentially on different regions, hence causing the development of the different heart structures (e.g., Roux,1895; Spritzer,1923).

Experimental results supporting both schools of thought have been presented. Studies in which portions of the early heart were reimplanted in a

different host showed that the heart developed normally, even though it experienced a different flow environment than its original position (e.g., Ekman, 1925). In 1932 Bremer described twin swirling blood streams from the vitelline veins as the factors responsible for the differentiation of the heart. However, Yoshida *et al.* (1983) revisited the flow patterns described by Bremer and found that the descriptions had been different than observed, thus discrediting Bremer's argument.

An important experiment arguing against the necessity of flow in heart looping is Manasek and Monroe's 1972 paper, which showed that in Hamburger-Hamilton (HH) stage 9+ chick embryos, blood flow is not needed for the looping of the heart. Chick embryos were placed in cultures, and potassium was added to block heart contraction. The authors observed that despite the absence of blood flow and heart contraction, the heart still began the looping process. In more developed chicks where the heart had already undergone early looping, the heart continued to loop. This seems to indicate that after stage 9 in chicks, flow is not needed for certain aspects of heart development. Although looping in the heart was shown to occur in the absence of both flow and heart contraction, one should take care to differentiate between form and function. That is, although the heart looped to a certain stage, the research does not imply that the heart was morphologically sound.

More recently, the idea that flow is indeed needed for normal heart function and development has resurfaced in experiments using avian (Clark *et al.,* 1984) models. Additionally, Sedmera *et al.* (1999) conducted two sets of

experiments on HH stage 21 chicks in which different vessels were ligated or constricted. To increase the afterload of the heart, the conotruncus was banded. The observed results included ventricular dilation, thickening of the myocardium, spiraling of the trabeculature, and the right atrio ventricular valve developing as a bicuspid valve instead of the normal tricuspid. Left atrial ligation, causing decreased left ventricle preload and increased right ventricle preload, resulted in hypoplasia of the left heart and compensation via growth in the right heart.

Another set of experiments blocking one of the vitelline veins in HH stage 17 chicks (Hogers *et al*., 1997) found that at later stages (34, 37, and 45) a large group of deformations was observed. These deformations included ventricular septal defects, semilunar valve analomies, atrioventricular anomaly, and pharyngeal arch artery malformations. This study, using dye to mark blood flow, concluded that flow patterns in the heart were significantly altered due to the vitelline vein blockage.

A recent study by Hove *et al.* (2003) makes a strong case that blood flow is necessary for proper heart development in the zebrafish. Hove *et al.* showed that blocking the flow of blood either into or out of the heart results in abnormal heart development. In this experiment, 50 um glass beads were implanted into the space between the yolk sac and epithelium of 37 hpf zebrafish embryos. In many of the fish, the bead ended up in the blood stream and was brought to the heart. The control fish were considered those in which the bead ended in a position near the heart, but did not affect the blood flow.

Fish in which the flow of blood was blocked demonstrated three characteristic phenotypes. First, their hearts had greatly reduced outflow tracts (i.e., bulbus arteriosus). In addition, the hearts did not loop. Finally, the walls of the inflow and outflow tracts collapsed and fused, beginning at 3 dpf. The similarity of the defects resulting from disrupting either inflow or outflow suggests that it is not the changes in transmural pressure in the cardiovascular system that is responsible, as the two different blockades should decrease (blocked inflow) or increase (blocked outflow) the pressure. Instead, the decreased shear force, the common feature of the two treatments, seems most likely to generate the developmental phenotype. These studies make a strong case that blood flow is a necessary factor for functional heart development in vertebrates.

Bartmann *et al.* (2004) argue that the lack of endocardial cushions observed by Hove *et al.* were not a result of lack of flow, but rather a lack of function, since many fish pharmacologically treated to prevent heart function still developed an endocardial ring.

Based on the previous body of data it appears evident that specific developmental windows in time enhance or decrease the sensitivity of vascular ECs to mechanical stimulation. The paucity of studies linking hemodynamics and development is most likely due to the difficulty of not only imaging blood flow *in vivo,* but making quantitative measurements as well. In order to better define these development windows, more precise and reversible methods for flow alteration are needed.

1.2.5 *In Vivo Flow Imaging*

Techniques such as ink injection (Bremer, 1932; Hogers *et al*., 1997) and microangiography (Yoshida, 1983; Weinstein *et al*., 1995; Weinstein, 2002) provide structural data and qualitative information regarding flow fields, but they do not provide the quantitative information required for detailed flow-structure interaction studies.

Quantitative flow data have been acquired using a suite of non-invasive methods. Ultrasound in chick embryos (Clark and Hu, 1982), zebrafish and mice (Phoon and Turnbull, 2003), particle tracking in the zebrafish (Schwerte and Pelster, 2000), and a novel use of fast confocal line scanning in mice embryos (Jones *et al.*, 2004) have been used to acquire blood velocity. These techniques are useful, but are limited to vessel size (small vessels for particle tracking and large vessels for ultrasound) or to making a measurement at a single point or radial slice.

Although better suited for studying structure due to slow scan times, MRI has been used to capture flow data inside the human heart (Kilner *et al.,* 2002), cerebral aneurysms (Tsuchiya *et al.,* 2004) and cerebral spinal fluid velocity through the foramen magnum (Haughton *et al.,* 2003). Using cardiac gated images, the flow throughout the cardiac cycle in these regions has been assembled. MRI is limited for use at scales approaching that of embryonic blood vessels because of its low spatial resolution.

In regions such as the embryonic heart where there is a large density of particles (blood cells) and rapid velocity changes, flow particle tracking and MRI will not work. A technique that can deal with these conditions is to study Digital Particle Image Velocimetry (DPIV).

DPIV is a whole-field, two-dimensional flow analysis technique that statistically follows groups of particles between pairs of consecutive images. Planar flow images are digitally acquired and stored. In software, each image is subdivided into many smaller, user-defined, interrogation windows. The Fourier transforms of corresponding interrogation windows are then cross-correlated, producing a peak corresponding to the average displacement within that window. By compiling all of the results from the individual interrogation windows, the velocity of the particles within the field of view can be calculated (Willlert and Gharib, 1991). Meinhart *et al.* (1999) have developed a technique for using DPIV in 30 um channels. The sizes of the channels used in their experiments are on the same order as those found in the embryonic heart chamber lumens.

In vivo DPIV has been limited to slower more external vessels such as rat and mouse mesentery vessels (Sugii *et al.,* 2002; Nakano *et al.,* 2003; and Koutsiaris *et al.*, 2004). The difficulty so far in utilizing DPIV *in vivo* has been the high blood flow rates in the larger vessels and heart. Optimal DPIV is performed when the particles being used are not blurred in the images. In the larger vessels, blood flow is too rapid for most microscope based imaging systems to effectively freeze the motion of the cells.

1.3 Objective and Organization

The formation of a functional heart is regulated by the coordinated interplay between a genetic program, fluid mechanical stimuli, and the inter- and intra-cellular processes that link them (Nerem *et al*., 1993; Takahashi *et al*., 1997; Taber, 1995; Hove *et al*., 2003). This process is genetically regulated at many different stages, including differentiation, migration, and pattern formation.

This study investigates the relationship between altered blood flow and altered heart shape and function. The goal is to develop a technique that allows for reversible, precise, and minimally invasive control of vascular blood flow. Additionally, *in vivo* quantitative flow measurements on the micron-scale existing in the zebrafish embryo were developed to map the resulting flow fields and correlate them to altered heart morphology. This work will allow us to quantitatively compare hemodynamic variables such as flow velocity and shear stress in both test and control fish. Furthermore, the heart morphologies resulting from different flow regimes should serve as strong evidence that blood flow is an important morphogen during vertebrate heart development

More specifically, the goals are to: i) apply a novel technique (DPIV) to the problem of mapping internal blood flow during development, ii) develop a technique for delivering and positioning small magnetic particles into the developing circulatory system, and iii) determine the effects of occluded and restarted flow on the major events of cardiogenesis.

Quantitative flow visualization will be accomplished through the use of state-of-the-art optical (high-speed imaging) and fluid-mechanical (digital particle

image velocimetry [DPIV]) techniques. The flow occlusion methodology presented herein is the result of a technology transfer from a fluid mechanical engineering application (Hayes *et al*., 2001) involving the use of micron-sized paramagnetic particles under the control of a custom-designed micro-electromagnet. Initial tests of this modified methodology are performed *in vitro* with controlled flow manipulations in capillary tubes and are then applied to an established vertebrate model organism, the zebrafish.

Chapter 2: Experimental Set-up and Methods

2.1 Introduction

This chapter is divided into 3 sections describing the experimental setups and methods utilized in our experiments. The first section deals with zebrafish handling. The second and third sections describe the imaging and injection methods, respectively.

2.2 Zebrafish Handling

Due to their numerous advantages, the zebrafish (*Danio rerio*) was chosen as our model (Fig.1). The imaging experiments were conducted at Caltech's Biological Imaging Center, which has extensive experience in working with zebrafish. Additionally, a dedicated zebrafish rearing facility houses wild type as well as different transgenic zebrafish.

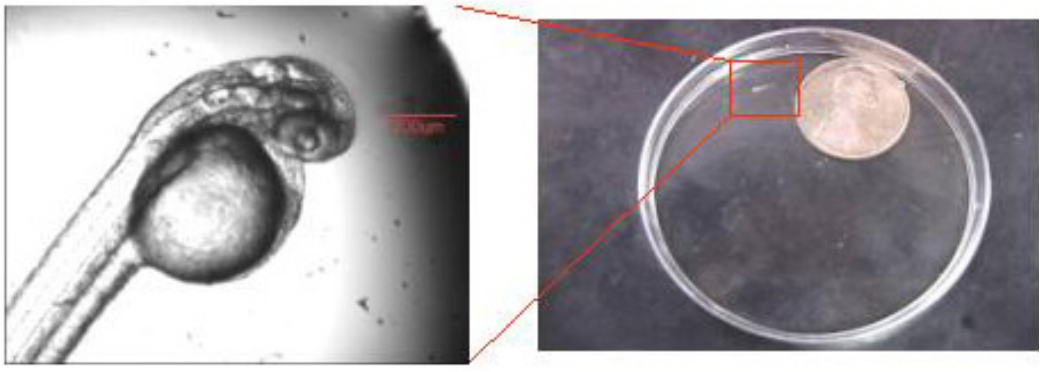

Figure 1: A magnified 37 hpf zebrafish embryo and the embryo to the left of a penny placed for scale.

As wild type fish are separated by sex, they are joined in smaller tanks for mating. Two females and one male are placed overnight in specialized breeding housing (Aquatic Habitats). The housing consists of two plastic tanks: a smaller tank sits inside the larger tank. Small holes on the bottom of the small tank allow eggs to fall into the outer container, safely away from the adult fish that may cannibalize them. A timer controls the lighting in the fish room, 14 hours of light and 10 of darkness, mimicking the lighting conditions during their springtime mating season.

The next morning, after the lights turn on, the adult fish are returned to their respective tanks, and any eggs are collected by pouring the contents of the outer tank through a tea strainer. The eggs are washed in a gentle stream of egg water (100X Egg water = 6g Instant Ocean sea salt in 1L distilled water) and are then transferred to a plastic petri dish and a solution of egg water with 1g/l of methylene blue for fungal inhibition.

Any dead embryos and waste products are removed from the dish to minimize bacterial growth, and the remaining eggs are rinsed several times to prevent fungal infections. The dish is then stored in an incubator maintained at 28.5 °C. At about 14 hpf the eggs are transferred to a solution of 30% Danieus Ringer with .003% phenylthiourea to prevent pigment formation and to make the fish optically transparent for several days. In the event that embryos are needed before 48 hpf, tweezers are used to puncture and remove the chorion to free the fish. Once free of their eggs, the fish are kept in 30% Danieus solution.

In all experiments requiring immobilization of the fish, the procedure was the same. Fish were anesthetized in a 0.02% solution of Finquel/tricane in 30% Danieus. Then, individually, the fish were transferred to a small vial of 1.0% ultra low gelling temperature agarose (Sigma) and then placed in a drop of agarose in a petri dish that has been chilled to 0 °C. Before the agarose hardens, the tip of an Eppendorf microloader is used to position the fish as desired in the drop of agarose (Westerfield, 2000). When using an inverted microscope, the fish are mounted ventral side down in a modified petri dish that consists of a 1cm diameter hole cut out in the center with a round slide-cover glued to the bottom of the dish over the hole (Fig. 2). The use of the cover slip provides a thinner surface and allows the fish to be mounted within the working distance of the objective lenses. In both cases, the agarose is allowed to harden and is then covered with a 30% Danieus solution with PTU and/or finquel.

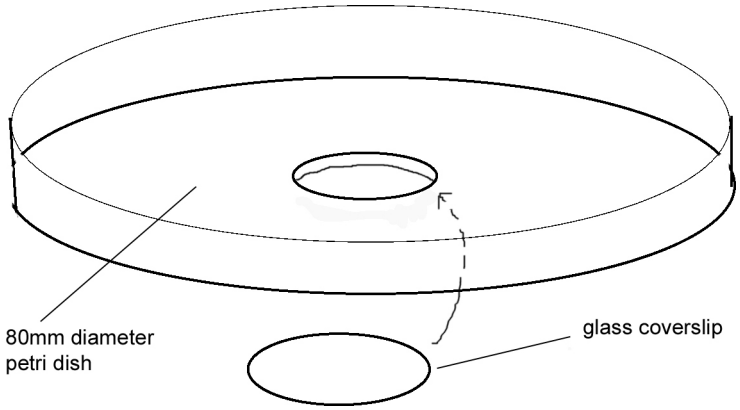

Figure 2: Modified petri dish for inverted microscopes

In experiments where the imaging only lasted a couple of minutes and no mounting was required, the fish were placed either in a drop of water or in non-

hardened agarose on a cover slip. The viscosity of the agarose was useful in slowing down the movements of the fish since they were not anesthetized.

2.3 Imaging Modalities

2.3.1 *Confocal Microscopy*

The first confocal microscope used in these experiments was a Zeiss LSM400. Fluorescent staining was performed in an effort to increase the contrast between the blood cells and the surrounding tissues. Embryos were soaked overnight in 0.001% Bodipy FLC5-Ceramide (Molecular Probes). The fish were washed several times in fresh Danieu's solution to remove excess stain and were then transferred to a new dish. After staining, the fish were mounted on the modified petri dishes to allow inverted confocal imaging. A computer running the Zeiss LSM software controlled the scanning, and a FITC filter set was used to allow the proper wavelength of light (505 nm) to excite the Bodipy stain. Images were acquired at 20 °C at the microscope's maximum frame rate of 0.7 frames per second, which is much slower than the cardiac cycle. The lower temperature, as compared with the incubator temperature of 28.5 °C, slowed the heart beat, providing more images per cardiac cycle. All images were stored on the computer, then transferred to a disk, and analyzed and processed using LSM software (Zeiss), Object-Image 2.05, Photoshop 5.02 (Adobe), and Freehand 8 (Macromedia).

2.3.2 *High-Speed CCD Cameras*

A) Dalsa

The high-speed imaging was performed using a borrowed Dalsa CA-D6-0256 (256 by 256 pixels) CCD camera and an EPix frame grabber housed in a computer running Windows 2000. The camera was mounted on the optical port of a Axiovert Microscope (Zeiss). Namarksi optics were used on the microscope to enhance contrast and provide thinner optical slices. The fish were imaged using a 10x objective lens at a frame rate of 440 fps. The high degree of apparent magnification is due to the camera's small imaging area. The images were stored as TIFs on the computer's hard drive. After collection, the images were transferred to a dedicated hard drive for permanent storage. The images were copied and converted to RAW files using Adobe Photoshop 5.02 for use in DPIV processing.

B) Kodak

Additional high-speed imaging was performed using a Kodak 1000HR high-speed camera that was mounted horizontally on a Nikon Eclipse TE2000-S inverted microscope (Fig. 3). The images were stored and processed as described above. To calculate blood cell velocities manually, the images from a given data set were imported as an image series and opened as a stack in ImageJ (NIH). The change in the position of a blood cell or particle from one frame to the next was measured, and since the frame rate and scaling factors are known, the distance and time of travel can be used to calculate velocity.

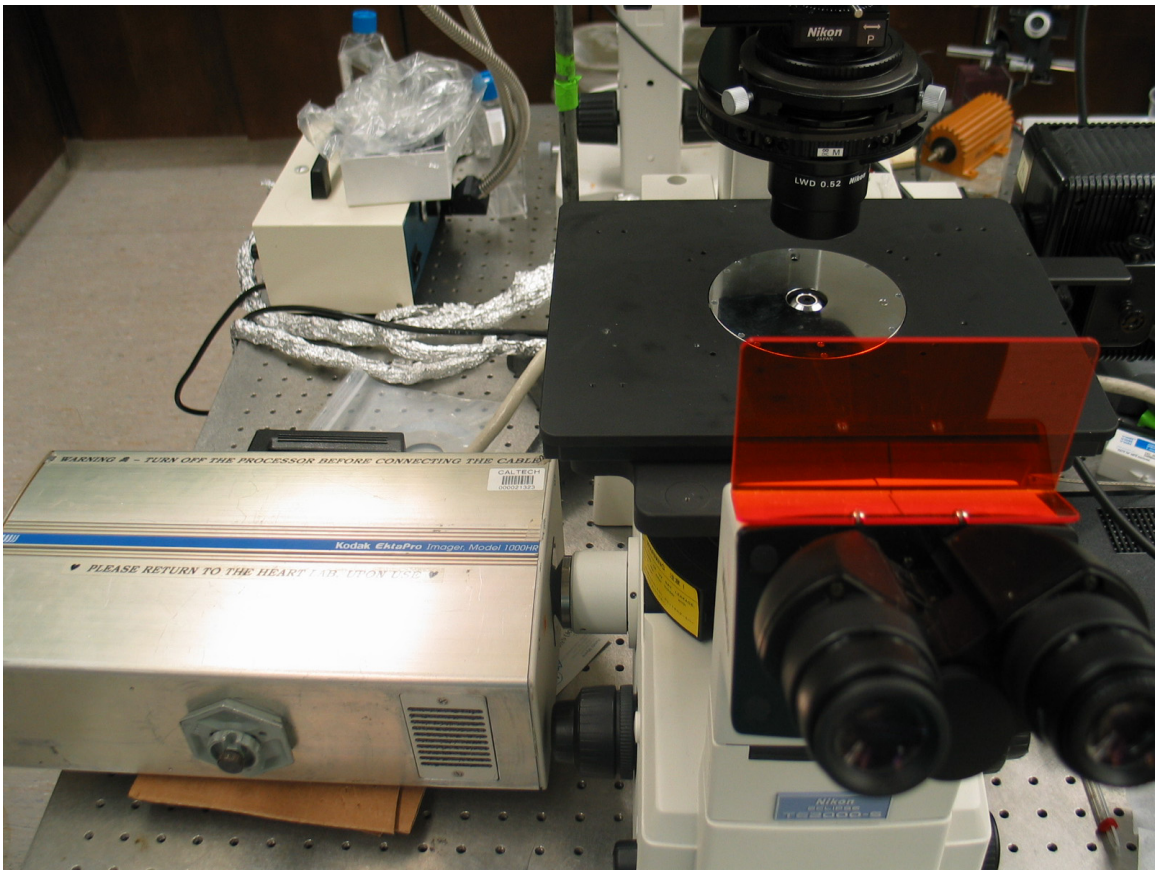

Figure 3: Kodak HRC 1000 on the left and Nikon Microscope on the right.

2.4 DPIV

The red blood cells in the images acquired from the Dalsa camera were used as the tracer particles in our standard DPIV software. Interrogation windows of 16 x 16 pixels with an 8 x 8 pixel overlap (50%) were used to reduce errors caused by out of plane motion and the movement of the surrounding tissues. DPIV analysis was performed on images acquired at 20, 25, and 28 °C. The intracardiac blood flow patterns appeared to be temperature invariant

across this range, although flow velocity did decrease slightly with lower temperatures (data not shown).

2.5 Injections

Twelve 48-52 hpf fish at a time were mounted, resting on their right sides, on one petri dish using the procedures described above. Injection needles, prepared using a Sutter Industries Laser puller with Plain Quartz microtubes (Sutter Instruments O.D. 1.0 mm, I.D. 0.70 mm, 10 cm length, Catalog #100-70-10) at the following settings: Heat 850, Filament 14, Velocity 20, Delay 110, Pull Strength 190, provided an effective tip for these injections. The micropipettes were backfilled with 3-4 ul of 250 nm PEG 300 fluorescent magnetic particles suspended in distilled water (Micromod, Germany) using Eppendorf Microloaders. The micropipette was then loaded into a General Valve PLC-100 Pico-Spritzer assembly and a micromanipulator. Tweezers were used to break off the tip of the micropipette at an angle as the sharper edge made injections easier. The open tip diameter was approximately 15 um as observed under a dissecting microscope (Zeiss Stemi SV 11). The petri dish was illuminated with a dual arm Zeiss KL 1500 LCD light source (Fig. 4).

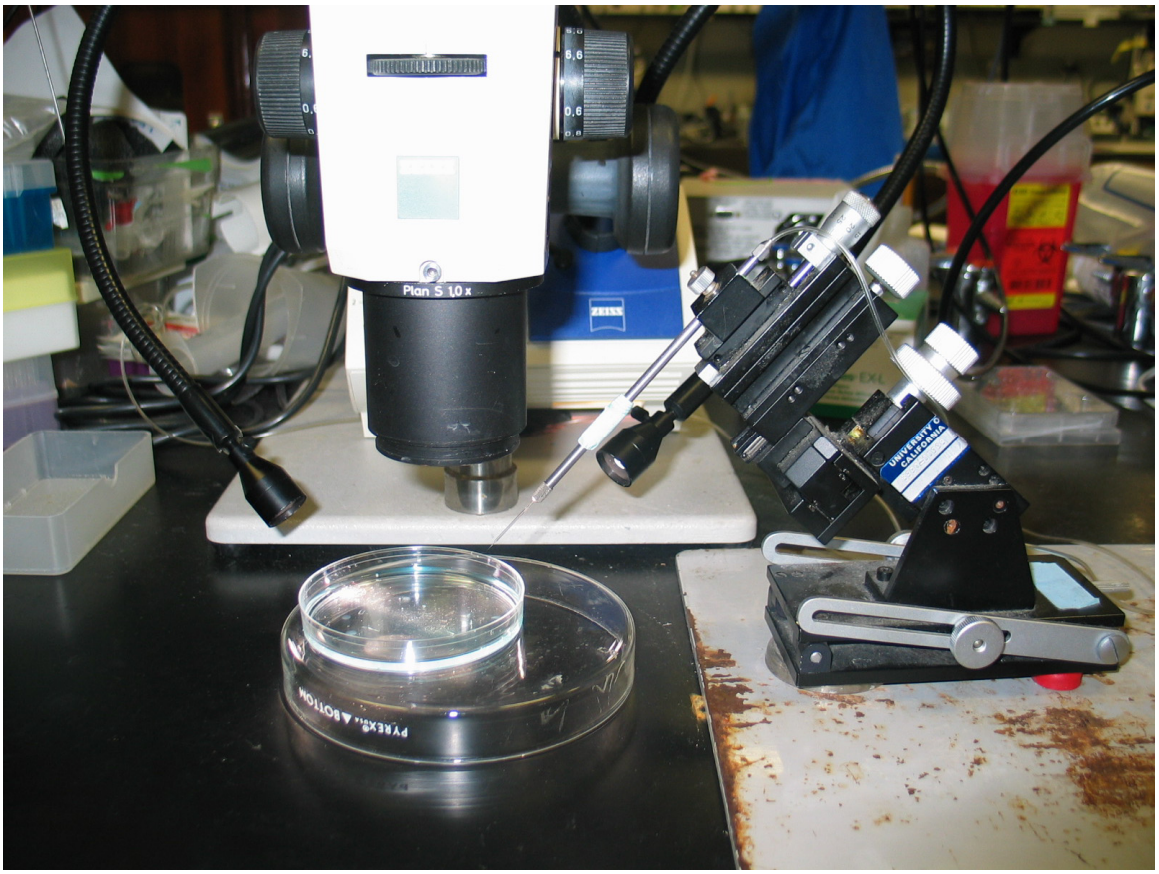

Figure 4: Microinjection setup with micromanipulator and micropipette on the right side of image.

Due to the difficulty in injecting solid particles into the vasculature, a custom protocol was developed. The balance pressure (P_{bal}) on the Pico Spritzer was increased to 0.2-0.3 PSI until the slug of fluid traveled down to the tip of the micropipette; it was then lowered back to 0.1 PSI. The tip of the micropipette was brought to rest against the dorsal artery near the middle of the embryo's tail. The pipette was withdrawn and the pressure was increased until there was a slow continuous flow of the magnetic suspension from the tip into the Danieu's solution in the dish. The tip was brought back to the fish, and then pushed through the epithelium and into the dorsal artery. Since the internal pressure of

the fish is higher than the ambient fluid, P_{bal} was raised to 0.3 or 0.4 PSI. When positioned correctly in the blood vessel, a small cloud of magnetic particles was seen to enter and travel along the blood stream of the fish. Only one successful injection was done per fish, in order to prevent excessive fluid volume from accumulating in the fish. Observation showed that within 15 minutes after injection, the magnetic particles settled above the yolk sac posterior to the heart and did not obstruct the flow.

In experiments where the fish were reoriented after injection, to provide better views of the hearts, the fish were removed from the agarose and remounted in a new drop of agarose, ventral side up. Danieus solution was added after the agarose hardened.

2.6 Miniature Electromagnet

Figure 5 shows the magnet, developed by Dr. Mladen Barbic of Caltech, used in these experiments. It consists of a 50 um soft-ferromagnetic (i.e., requires low relatively weak magnetic field to become magnetized) core, wrapped with 25 um diameter magnetic wire. The tip is sharpened by electro-chemical etching (Barbic, 2001). This assembly is mounted on a small chip, with two leads attached to the core windings allowing for connection to external power sources. The small tip size increases the field gradient, allowing for a stronger force to be exerted on magnetic particles.

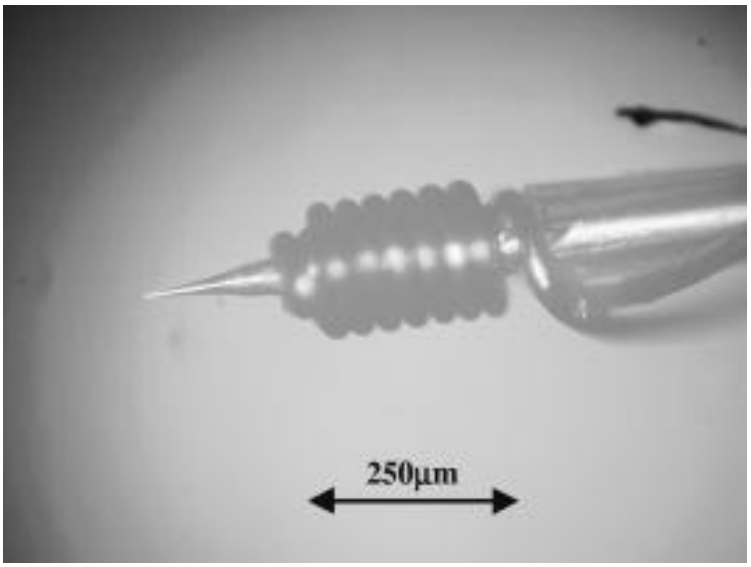

Figure 5: Miniature electromagnet. 50 um soft-ferromagnetic core is surrounded by two sets of 25 um magnetic wire windings.

The magnet was held by an alligator clip attached to a wooden rod that in turn was held by an electrode holder (WPI). The entire assembly was mounted onto a micromanipulator as shown in Figure 6.

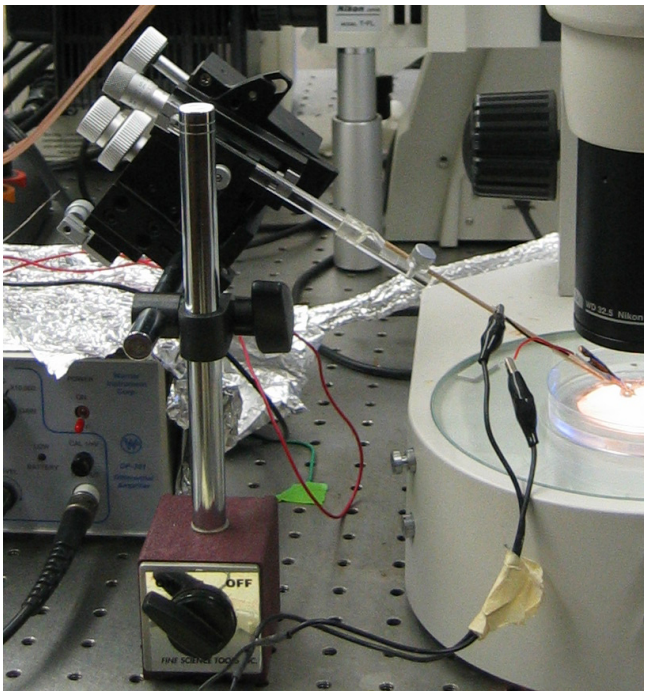

Figure 6: The magnet setup. The magnet is at the end of the wooden rod. The whole assembly is controlled by a 3-axis micromanipulator.

A Kepco Bipolar Operational Power Supply/Amplifier was used to supply the current to drive the magnet. A simple circuit, shown in Figure 7, containing a 156 Ohm Power Resistor with a 500 W rating, used to prevent resistor break down by overheating, provided a constant current to the magnet. The amplifier was run in voltage control mode, with the voltage set at approximately 50 V. This resulted in a current of 320 mA, well above the 100 mA at which the magnet was calculated to exert a force of 10 pN on 1 um magnetic particles (Barbic, 2001), and well above the estimated drag forces on the particles due to blood flow (1pN).

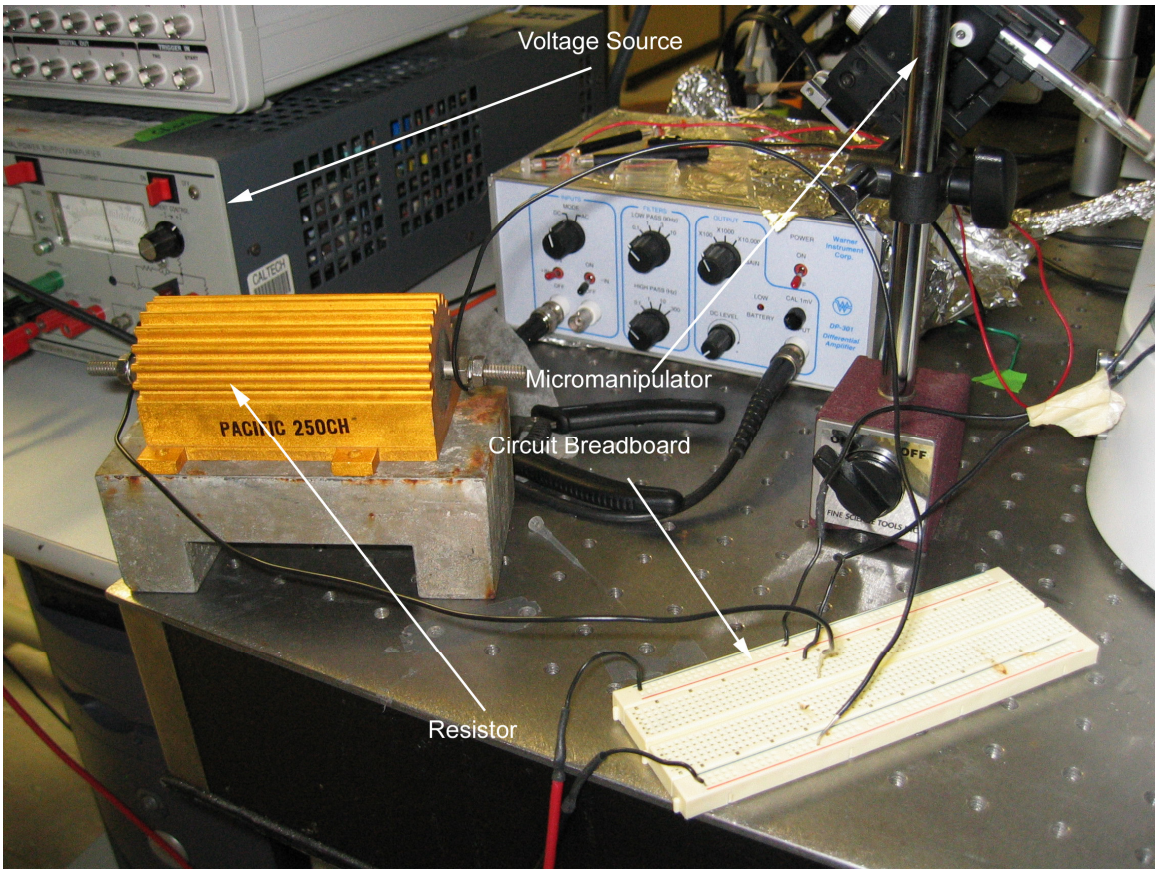

Figure 7: The different components of the circuit to drive the electromagnet.

2.7 *In Vivo* Magnetic Particle Control

The entire dish was placed underneath the Nikon SMZ1000 dissecting scope. The micromanipulator/magnet assembly was positioned near the stage of the microscope and arranged such that the tip of the magnet came in contact with the fish as shown in Figure 9.

Figure 8: The electromagnet is brought up against the fish near the heart.

To prevent any current spikes from damaging the magnet, only one lead of the magnet was connected to the circuit before the voltage source was turned on. The magnet was positioned such that the tip of the magnet was touching the fish along the ventral centerline. The particles that had settled out of the blood stream tended to collect on either side of this centerline. When the magnet was placed on the fish, the particles migrated towards its tip; by moving the magnet slowly on either side of the centerline, a small bolus of particles was formed. In intervals of approximately 5 minutes, the magnet was moved towards the inflow

of the heart. When the flow was blocked, the blood cells began to accumulate upstream of the blockage and on the sides of the yolk sac.

Once the bolus was in place, to minimize particle absorption into the tissues, the voltage was reduced from 50 V to approximately 25 V thereby reducing the current and magnetic field strength.

The methods described in this chapter were used to visualize the blood flow inside the fish and to control the position of magnetic particles within the blood stream.

Chapter 3: The Use of Confocal Microscosopy for *In Vivo* Flow Imaging

3.1 Introduction

This chapter discusses the use of confocal microscopy to image intra-cardiac blood flow and heart morphology during zebrafish development.

3.2 Experimental Conditions

4.5 dpf fish were stained and mounted as described in Chapter 2. An appropriate filter set (FITC) and the maximum frame rate of the confocal microscope (0.7 sec per frame) were used to acquire the images. Initially, it was thought that the Bodipy Ceramide, with its relatively high permeability into living cells, would stain the red blood cells along with the membranes of the heart, allowing the cells to be used as tracer particles for the flow. However, the opposite occurred, with the serum taking up the dye. The procedure was similar for the high-speed CCD experiments, but no staining was performed.

3.3 Confocal Imaging Results

Laser scanning confocal microscopy was used to obtain a general map of the heart and the resulting flow. At the maximum scan rate of 0.7 sec per frame, the blood flow was too fast to freeze the individual cells in motion resulting in black streaks in the fluorescent serum (Fig. 10). However, these images provided

excellent heart structure information and a qualitative map of the intracardiac flow field.

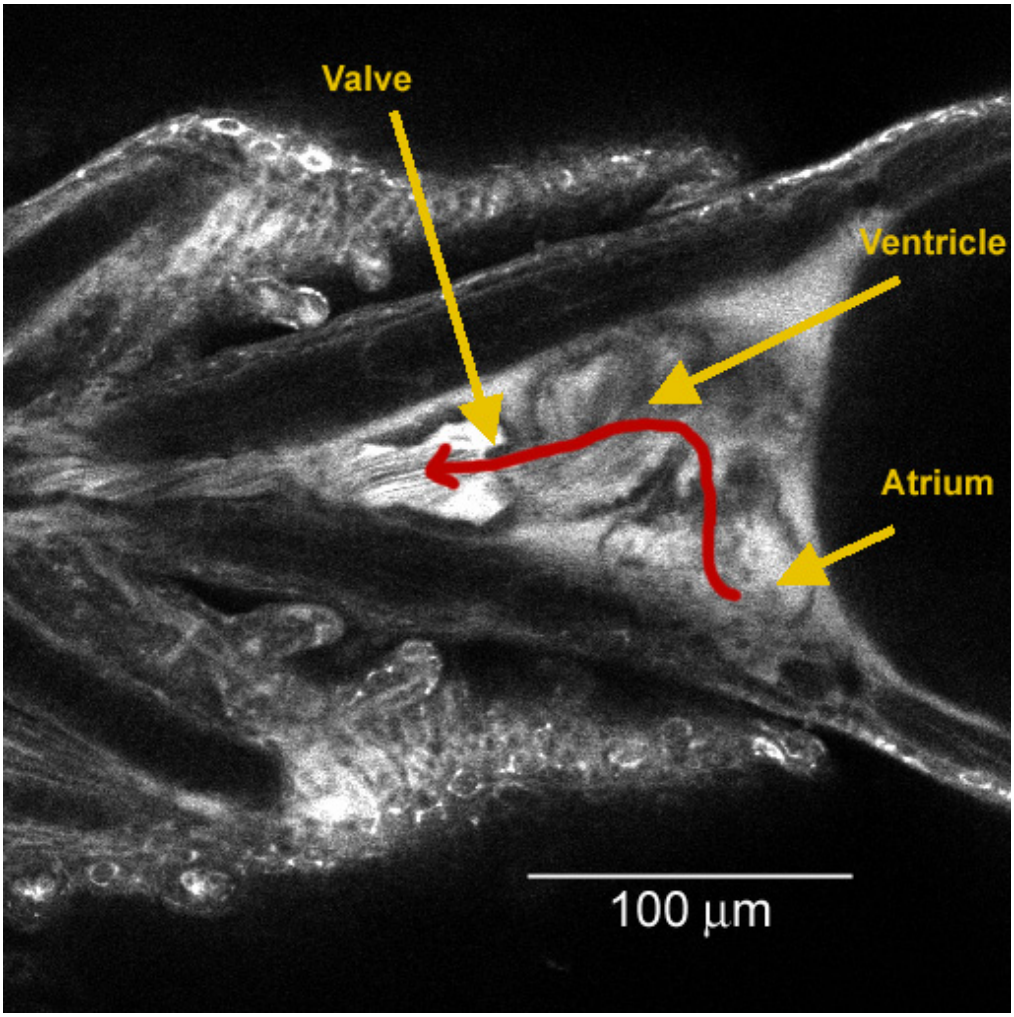

Figure 9: Confocal image of the 4.5 dpf heart during systole. The serum appears white in the image.

Given the small size of the heart, with a length of approximately 150 um and a Reynolds number less than 1 (0.02), implying that the ratio of viscous forces to inertial forces is very large, such a dynamic system was unexpected. The long streaks observed in the image indicated a relatively high blood velocity since the particles traveled across the image in the time it took to scan. The

presence of circular white patterns near the valve also suggested regions of vorticity just downstream of the ventricular valve. Due to the slow scan time relative to the cardiac cycle, the series of images were not acquired in consecutive phase order and were sequentially ordered manually. The resulting image sequence showed that the heart contractions themselves were extremely dynamic. An ejection fraction systole of approximately 60% was calculated by fitting a curve to half of the projection of the heart at end diastole and end systole. Then making the assumption that the heart was symmetric about this line, the volume was calculated by rotating the curve about the symmetry line. The ejection fraction was the difference in the two volumes.

Despite our inability to extract quantitative information, the images showed the presence of an extremely dynamic and complex flow environment, with the formation of a jet between the atria and ventricle and between the ventricle and bulbus. Furthermore, based on the confocal microscope images, the V-B valves were shown to be present and functioning at this stage and were subjected to regions of vorticity on their downstream surface. Figure 11 shows a representational image with the vorticity calculated from the DPIV analysis superimposed on the confocal image. The relatively high velocity implied by the streaks in combination with the small size of the heart and viscous blood suggests a high shear environment in the heart.

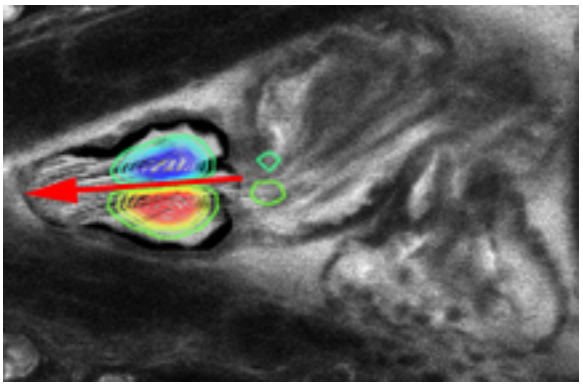

Figure 10: Hybrid of DPIV and confocal laser scanning microscopy results, representing the region of vorticity just downstream of the V-B valve. The reddish circles imply counter-clockwise vorticity and blue represents clockwise vorticity.

Chapter 4: *In Vivo* Flow Analysis

4.1 Digital Particle Image Velocimetry

Digital Particle Image Velocity (DPIV) is a whole-field, two-dimensional flow analysis technique that statistically correlates groups of particles between pairs of consecutive images. Developed initially as a diagnostic quantitative flow visualization tool for the field of fluid mechanics, the use of DPIV has spread to many different branches of fluid dynamics since its development over 10 years ago.

DPIV experiments are conducted by seeding a flow with small neutrally buoyant particles. The particles are selected such that they both follow the flow patterns and do not alter the flow properties. For experiments using liquids, small (10-100 um) reflective or fluorescent particles are used, while for gas experiments, oil or alcohol droplets are often used. These particles are typically illuminated using a planar light sheet, and sequential images are acquired of the flow. These images are acquired with a CCD camera, which sends them to computer memory. The images are in turn processed using the DPIV software. The key to illumination and acquisition is to provide high contrast between the particles and the background, freeze the motion of the particles in each image, maintain short time between images so that particles do not move out of the area of interest, and avoid regions of high three-dimensionality in the flow.

The rapid exposure time necessary to freeze the image has been achieved with mechanical shutters in front of the camera, and more recently by

asynchronous frame triggering of a CCD camera in conjunction with pulsed lasers. Improvements in CCD data transfer rates have allowed for the use of DPIV in higher velocity flows than initially possible. The width of the laser sheet can also be controlled to some degree to allow some flexibility in any 3-D movements of the particles.

In processing the data, sequential pairs of images are compared. Each image is divided into smaller interrogation windows. In contrast to particle tracking, DPIV statistically follows patterns of particles from one image to the next. Using the intensity or gray levels of the particles, the two-dimensional cross-correlation is calculated. The peak value of the cross-correlation corresponds to the displacement and direction that gives the best overlap between the particles in the two images. Since the time between images is known, this displacement vector is easily converted into a velocity vector. By repeating this process for each interrogation window, a vector field map of the flow area is produced.

In order to optimize this process, several conditions must be met. First, the introduction of the particles should not alter the properties of the flow. Secondly, there should be enough particles to provide a high degree of accuracy in the calculations. Additionally, the interrogation windows should be small enough to minimize any velocity gradients, yet maintain enough particles (5-7) within each window to lower the error in the statistical calculation.

DPIV differs from particle tracking in that the software is not following individual particles from frame to frame. Rather, the software is following

statistically groups or patterns of particles. The advantage of this method is that the entire flow field has markers with which to analyze the flow; there are no voids. However, the high number of particles makes it difficult and tedious to perform these calculations by hand. The density of the particles is a balance between leaving no voids, yet not having a density so high that the particles begin to overlap each other. Figure 11 below shows representative densities of particles for three different flow analysis methods, particle tracking, DPIV, and laser speckle velocimetry (LSV). Figure11a shows what a reasonable concentration of particles for particle tracking could be. Due to the low number of particles, it would not be overly tedious to manually track these particles from one frame to the next. Figure 11c shows the density typical of LSV. In this technique rather than follow groups of particles, the software follows “speckles” of light and dark regions. With the overlapping of particles, DPIV would have a hard time calculating a meaningful cross-correlation due to the overlapping pixel patterns.

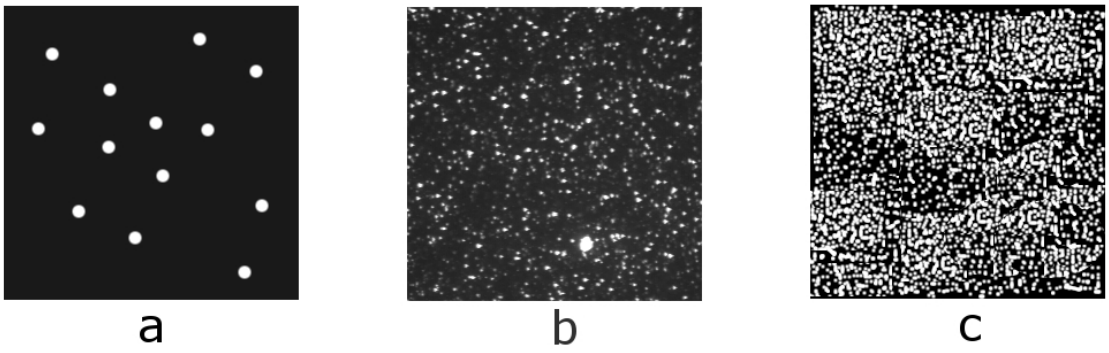

Figure 11: The three modes of particle density. The white points represent the tracer particles. A) A low density of particles is appropriate for particle tracking. B) A high concentration with no overlapping of particles for DPIV. C) A higher density of particles is used for laser speckle velocimetry (LSV).

Another factor to optimize the accuracy of DPIV is setting up the interrogation windows so the shift of particles from one frame to the next is not greater than approximately one quarter of a window length (Gharib and Dabiri, 2000). Under this constraint, the majority of particles in the first image are still present in the second one, a small portion have either left or entered the windows. For example, using 16 x 16 pixel windows, the average displacement should not be larger than 4 to 5 pixels. Further techniques such as slightly shifting the interrogation window itself from one frame to the next can be used to maintain a sufficient number of particles within the interrogation region. Also, outlier removal and other error detecting schemes are normally implemented (see Gharib and Dabiri for more details).

In order to save computational expense, instead of performing all the addition required of the cross correlation in the spatial domain, the FFT (Fast Fourier Transform) of the spatial information is performed, and the complex conjugates are multiplied. The inverse FFT is performed on the product, and the output produces a velocity vector in the spatial domain. For a window of N pixels by N pixels, this results in N^2LogN calculations as opposed to N^4 calculations in the spatial domain. The calculations can further be reduced by taking advantage of the symmetry of the FFT (Willert, thesis). By compiling all of the results from the individual interrogation windows, the flow properties within the field of view can be calculated (Willlert and Gharib,1991). For a deeper mathematical description of DPIV, Willert and Gharib (1991), as well as Westerweel (1993), provide excellent references.

4.2 Micro-PIV

With the increase of MEMS devices aimed at biological use, interest in mircofluidics has increased. The application of DPIV at such small sizes has not been a simple adaptation. Along with the normal constraints on performing DPIV, and additional set of problems are encountered at the smaller length scales. One of the difficulties in microPIV has been the selection of particles. Particle selection is not immediately obvious, because there is a need for enough particles to seed a flow in sub-millimeter channels, yet they should not be overly subject to the effects of Brownian motion, which would add random movement to the particles. Additionally, the typical laser-sheet illumination method is not as easy when the flow chamber is placed underneath a microscope. Since the flow chambers are so thin, the entire flow volume is illuminated by the laser sheet, so extra care must be taken to account for any visible 3-D effects. Devasenathipathy *et al.* (2003) have managed to lessen the restrictions of the above problems by performing microPIV in microfabricated 100 um wide channels in which dual Nd:Yag lasers were used to illuminate the motion of 500 nm fluorescent particles using a fiber optic cable to localize the illumination. The images were captured using a cooled CCD camera. A combination of PIV and particle tracking (Takehara *et al.*, 2000) was used in the analysis to provide higher resolution results. The techniques used in these experiments may lend themselves to straight and non-moving biological systems.

4.3 *In Vivo* DPIV

As mentioned in earlier chapters, there is strong evidence suggesting that blood-flow induced forces play a role in vertebrate heart development. However, in order to better understand any interplay between flow and development, a means of analyzing the intra-cardiac flow field must be developed. As it stands now, analysis of the intra-cardiac flow field is limited to qualitative methods only.

One of the goals of this thesis is to develop a method of using DPIV for *in vivo* flow analysis. There has been some use of DPIV for analyzing the flow of blood in straight, slow moving surface vessels, such as the arterioles in the mesentery tissue of rats (Sugii *et al.*, 2002). Use of DPIV in deeper tissues and more complicated flow has not yet been performed. The constraints on microDPIV are further compounded when working with an *in vivo* model. Along with the issues of particle selection, optical accessibility, and moving boundaries are other factors that must be addressed.

The hypothesis for this project is that a combination of microscopy and digital imaging will provide images suitable for *in vivo* DPIV. We choose the zebrafish (*Danio rerio*) as our model due to the optical accessibility and rapid development time. We commence with a laser scanning confocal microscope and then use CCD cameras and Nomarksi optics to acquire images.

Following our use of confocal microscopy as discussed in Chapter 3 we switched over to the use of CCD cameras. A Pulnix 9701 TM CCD camera was connected to the camera port of an inverted compound microscope (Zeiss Axiophot) and used to acquire images of the blood flow in a 4.5 dpf zebrafish

embryo. However, the maximum frame rate of 30Hz was too slow to freeze the image of the cells in each frame, so a faster camera was required.

A high-speed CCD camera (Dalsa CD-D6-0256) was next used. To support the weight of the camera on the vertical camera port, ropes were hung from the ceiling and passed underneath the camera. The camera was connected to an Epix frame grabber in a computer running Epix software (XCAP v.1.0). The embryos were mounted in agarose as previously described and imaged at room temperature. Nomarski optics were used to enhance the contrast and provide thinner optical sectioning. This resulted in a reduction of the amount of light passing through the embryo so the maximum illumination setting of the microscope was required. Due to the vertical positioning of the camera some data collection runs were not useable because of a slight “rocking” of the image due to camera shake. Side ports such as those found on the Nikon were easier to use. A frame rate of 440 frames per second (fps) successfully froze the movement of the blood cells in each frame. Figure 12 shows images acquired using the technique above, with the different heart chambers and blood cells labeled for identification.

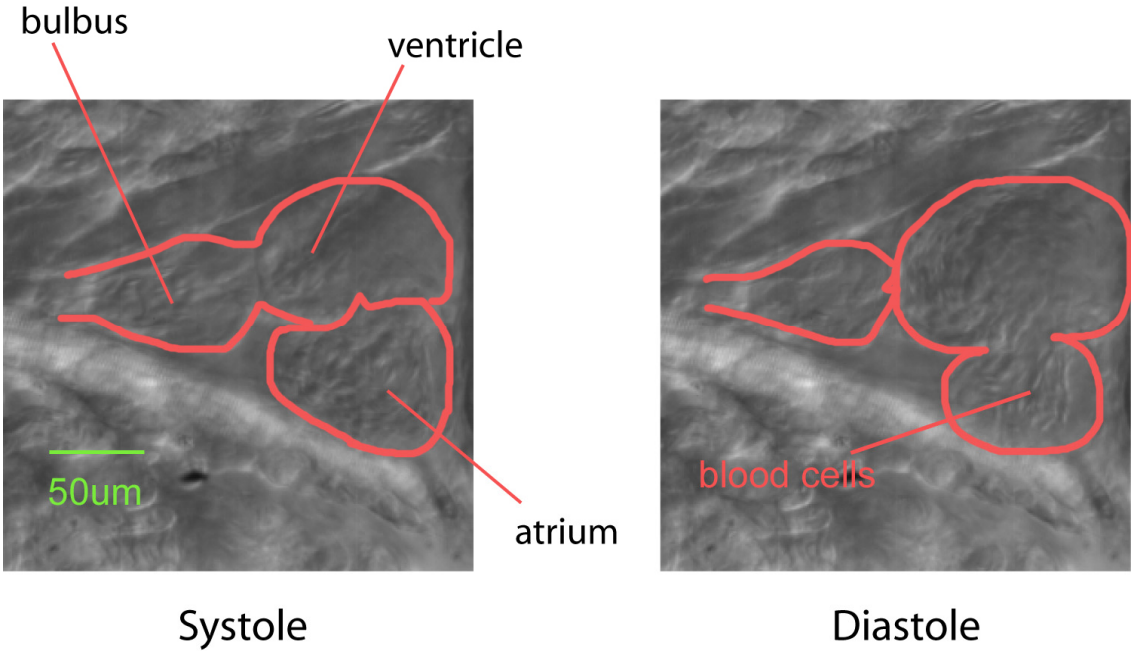

Figure 12: Two frames from the data set showing systole and diastole of the 4.5 dpf heart. The red contours are the heart lumen boundaries.

At this frame rate, individual blood cells were distinguishable, and the different cardiac phases (e.g., systole and diastole) were evident. Imaging was set up to maximize the focus on both the A-V and V-B valves. For the heart, a magnification provided by a 10x objective lens seemed to provide the best compromise between resolution and a large enough viewable area to capture the entire flow field. It should be noted that the magnification required depends on the camera and the microscope being used. The Dalsa has a 256 x 256 pixel sensor, and in combination with the camera port on the Zeiss microscope, the heart filled the field of view with a 10x objective. However in later experiments using a Kodak high-speed camera, a 20x objective was required to view the same area.

4.4 DPIV Settings

Based on the image size of 256 x 256 pixels, an interrogation window size of 32 x 32 pixels with a 50% overlap was initially chosen. However, it soon became evident that the window size was too large for the heart lumen, since the windows extruded quite a way into the surrounding tissues and additionally did not provide many vectors for the results. Window sizes of 16 x 16 and 8 x 8 were subsequently used. In the end the 16 by 16 windows were finally chosen. Disturbingly, the peak velocity calculations changed according to the window size. Manual particle tracking was used to calculate the velocities presented below.

The results of the DPIV processing confirmed the qualitative data obtained using the confocal scanning images. The resultant velocity vectors demonstrated the existence of jets through the V-B and A-V valves and regions of vorticity downstream of the valves during both diastole and systole (Fig. 13).

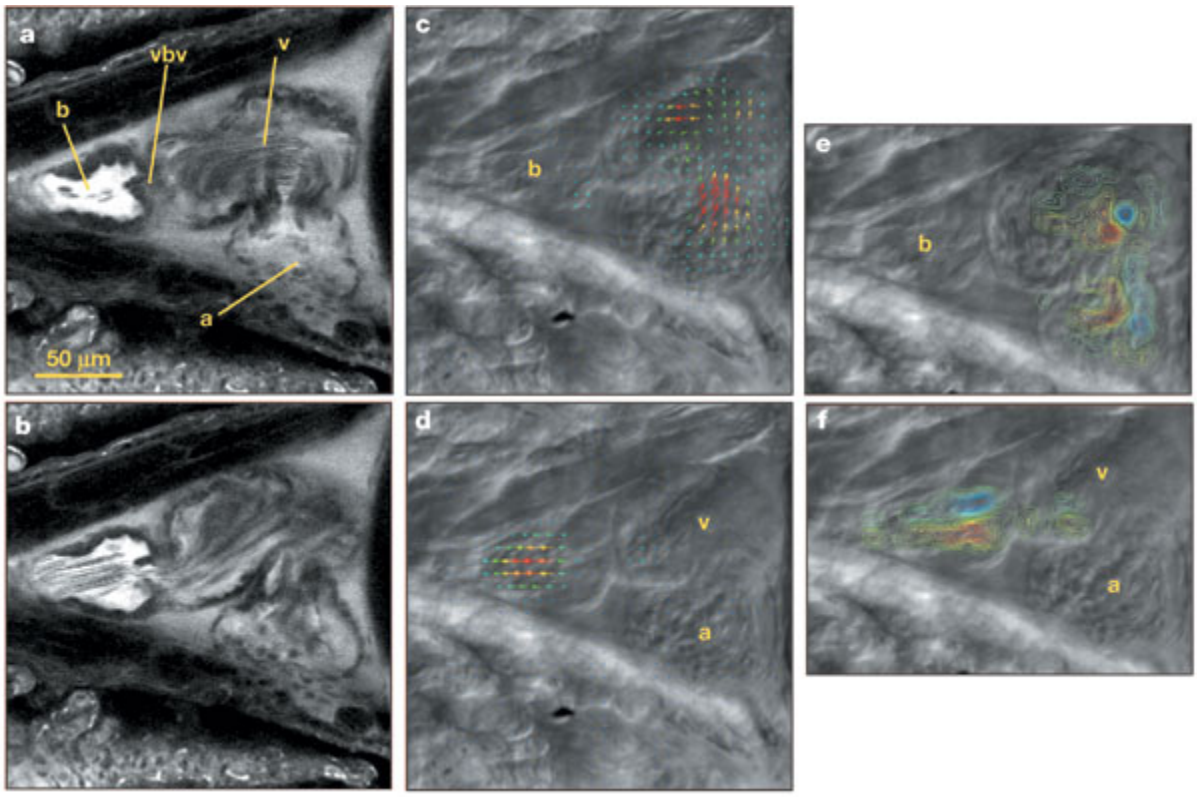

Figure 13: Comparison of confocal images and resultant DPIV from high-speed CCD images. (b=bulbous, v=ventricle, a=atrium, vbv=ventriculu-bulbar valve) First row (1a,c,e) shows the heart during diastole. 1c shows the DPIV vector field, and 1e shows the vorticity field for the same data. The second row shows the same fields but during systole. (*From Nature 412: 172-177***)**

4.5 Results

Resulting velocities from the images acquired using the Dalsa high-speed camera between the atrium and the ventricle were calculated to be 0.5 cm/sec. Shear stress is defined as the partial derivative of the flow profile, $u(y)$ perpendicular to the direction of flow. For example, for a two dimensional flow profile traveling along the x-axis, with height along the y-axis, shear stress would be calculated by:

$$\tau = \mu \frac{\partial u(y)}{\partial y}.$$

For the shear stress calculations through the V-B valve, a no-slip linear flow profile, $u(y) = \frac{U}{h} y$, where h is vessel radius, was chosen since the flow from the atrium to the ventricle does not have time to fully develop. This results in a shear of

$$\tau = \mu \frac{U}{h}.$$

There are no exact numbers for the viscosity of the blood in the zebrafish since there is not enough blood to perform normal viscosity measurements. Further complicating the measurement, the viscosity of blood is dependent on velocity, hematocrit (blood cell concentration) and strain. Given the relatively large size of the vessel under examination and the relatively high velocity flow, μ was assumed to be constant at 5×10^{-3} N·s·m^{-2}, roughly 5 times that of water. This number may be slightly incorrect, but since shear stress scales linearly with viscosity, a small change in viscosity would not cause a large change in the shear stress. The shear stress on the wall at the A-V valve was calculated to be over 70 dynes/cm^2, well over the 0.2 dynes/cm^2 needed for endothelial cells to sense. We also did tests at 25 and 27 °C and found similar flow patterns, with a negligible increase in velocity.

To ensure that the shear results are not largely dependent on flow profile assumptions, the wall shear stress for a fully developed flow as well as a

partially developed flow were calculated and found to be higher than a linear flow profile (Appendix A).

4.5.1 37 hpf fish

The success in imaging the 4.5 dpf fish, and the high shear rates encountered, encouraged us to study the flow in the 37 hpf embryo. At this stage the atrium and ventricle are aligned in a tube-like configuration, the bulbus is not present, and the valves have not yet developed. Due to the orientation of the heart at this stage, only the inflow of the blood to the heart over the yolk sac was visible (Fig. 14a). As the velocity at this stage and location is much slower than the flow in the 4.5 dpf heart, the Pulnix CCD camera with its 30 Hz frame rate was sufficient to freeze the individual blood cells in motion.

DPIV was performed on the acquired images, and the results captured the flow over the yolk sac and into the heart (Fig. 14b). The erythrocyte velocities were calculated to be 0.5 mm/s. With this velocity and the vessel dimensions, the wall shear stress was calculated to be 1 dyne/cm^2. Previous literature has set the shear sensitivity threshold of *in vitro* endothelial cells at 0.2 dyne/cm^2 (Olesen, 1988), which implies that the endothelial cells in the primitive heart may respond to the shear stress imparted upon them by the blood flow.

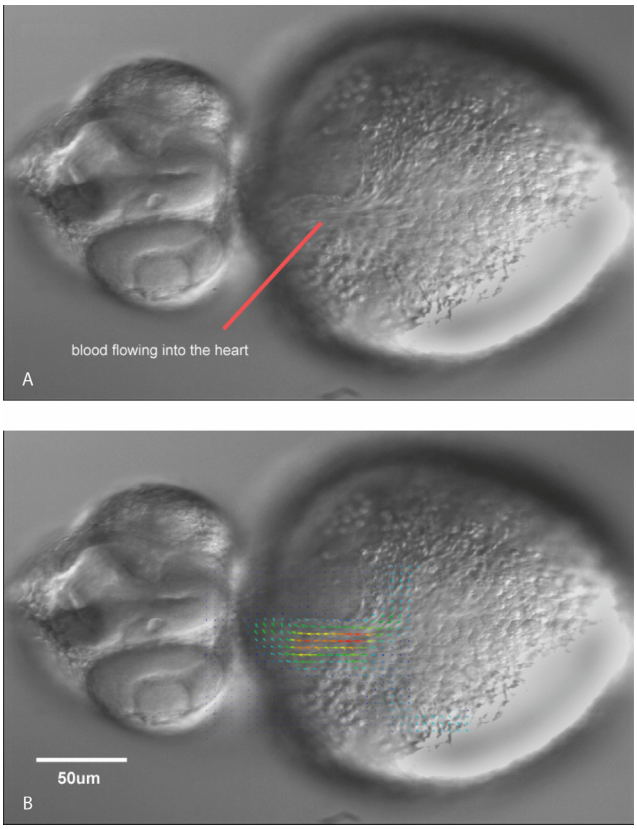

Figure 14: A) The original image of the 37 hpf embryo showing the blood flow over the yolk sac. B) DPIV results superimposed over the original image showing the relative velocities of the flow (red is highest velocity, blue the slowest).

4.6 Manual Processing

As mentioned above, due to inconsistencies in DPIV velocity calculations, manual particle tracking was used to calculate velocity values. Even with an acquisition rate of 440 fps, comparing sequential images proved difficult. During the peak flow periods, many blood cells appear blurred into the surroundings and may be traveling out of the plane of view. The gray on gray images make it difficult to be sure if a cell has moved along the path of flow, or whether a new cell has just entered the plane of view. It is interesting to note, that when playing

the images back as a movie at 30 fps, the flow and cells appear obvious, yet when going frame by frame it is not so clear. Roughly 10 pairs of images during peak systole were examined for pairs of cells that could be tracked. On average, there were about 5 cells that could be followed between two images. The issue of focus is paramount, and the inherent lack of contrast in these images is not optimal.

These results demonstrate the first use of *in vivo* DPIV. The use of particle tracking and DPIV calculated relatively high velocities and extremely high wall shear stress in the 4.5 dpf fish. Furthermore, levels of shear stress in the 37 hpf fish were calculated to be well above the experimental minimum that cultured cells can detect. These results suggest that the forces imparted by blood flow on the heart lumen are large enough to cause an endothelial cell response, which in turn increases the probability that hemodynamic forces play a role in early vertebrate heart development

4.7 Problems

Despite the novel results discovered using DPIV and particle tracking, there are some problems that need to be overcome to improve future use of *in vivo* DPIV. These include a lack of contrast between the blood cells and the surrounding tissues, moving boundaries, and blood cell size relative to the vessels. As mentioned previously, the peak velocity calculation varied according to the interrogation window size. For comparison the same images were processed using 32 x 32 windows, 16 x 16 windows, and manual particle

tracking. The manual tracking resulted in a peak displacement (from one frame to the next) of 7 pixels, while the 32 pixel windows resulted in a peak displacement of 3 pixels and the 16 pixel windows with a displacement of 5 pixels.

The inconsistency in the velocity calculations is likely due to several of the problems mentioned above. Perhaps the most important factor is the large size of the blood cells relative to the heart lumen. This large size makes interrogation window selection difficult. We wish to obtain the optimal five to seven particles per interrogation window, yet making the windows larger creates further problems by including the heart tissues in the calculations and allowing for velocity gradients. As mentioned earlier, the moving boundaries of the heart can show up as velocity vectors and skew the analysis and further calculations.

The lack of contrast between the cells made particle tracking difficult as well; it was often difficult to tell where a cell had moved from one frame to the next. The few cells that could be tracked from one frame to the next did not provide a sufficiently large data set.

4.8 Attempted Solutions via Image Processing

In an effort to increase the contrast of the images, several different image processing methods were used prior to DPIV and manual tracking operations. Edge detection was first used to see if it became easier to follow individual cells from one frame to the next. However, it became evident that defining the edges did not solve the problem of identifying corresponding cells from one frame to the

next. Edges appeared as light rings against a dark background. However, because of gray on gray images, many objects that were not cells also appeared as rings or lines. This method was not compatible with DPIV since it requires localized discrete points, not rings (Fig. 15).

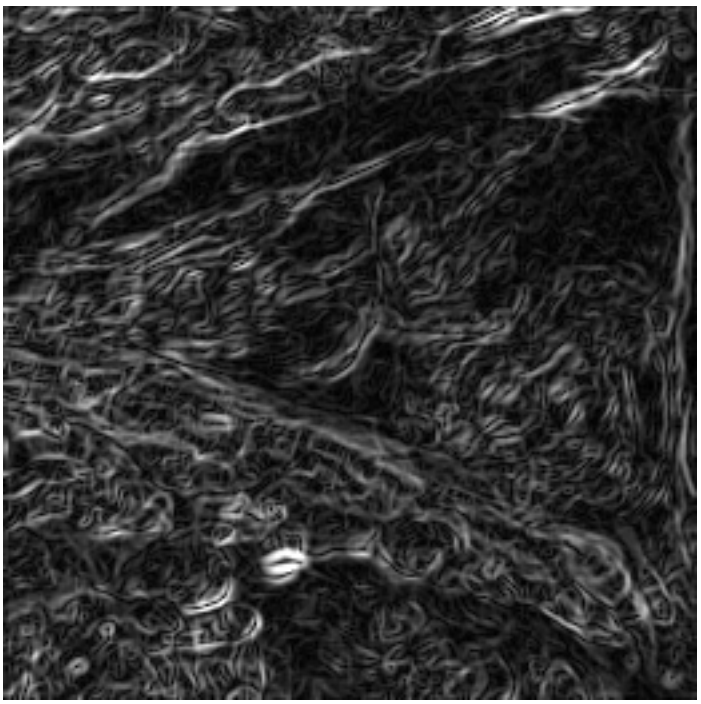

Figure 15: Image of systolic phase passed through an edge detection filter in an attempt to enhance cell contrast.

The last method used was to perform DPIV and particle tracking on the differences between images. When performing this operation, only the differences between the two images show up on a black field (e.g., if you subtract an image from itself you end up with a black field). The expectation was that differences in cell movement would register as the only points in the differenced images. This worked in some images (Fig. 16a), but in other pairs there was

movement of the entire region from one frame to the next (Fig. 16b), making it un-useable for DPIV. Schwerte and Pelster (2000) had better success using this method in the blood vessels, rather than the heart, of the zebrafish since they do not tend to move as much.

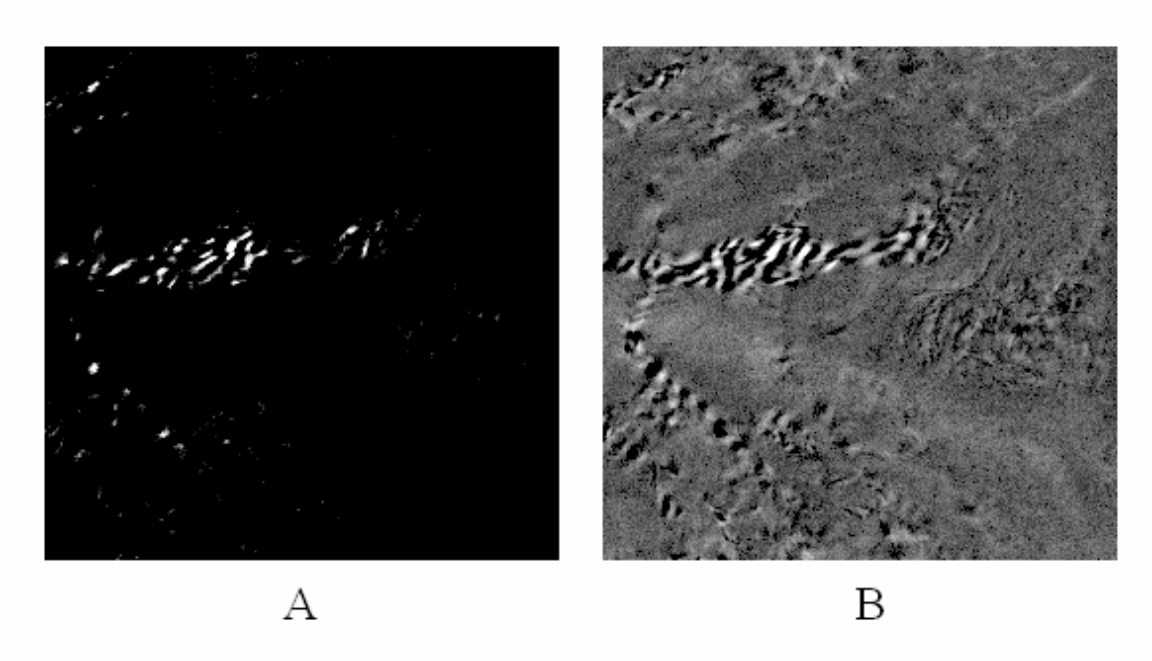

Figure 16: (A) Difference between images 117 and 116. The white points represent the movement of the blood cells. B) Difference between images 119 and 118. The gray background indicates that the background has moved between the frames. The variability between pairs of images makes this process unsuitable for DPIV analysis.

These methods suffered from the fact that the fish heart is not a rigid environment. The walls move and change the lumen shape. Therefore there is more motion than just the particles to subtract or average, resulting in “difference regions” in the tissues that further complicate calculations. The lack of contrast

also plays a role in the difficulty of tracking individual cells. If the contrast were sufficient to better distinguish between the cells and the surrounding tissues and fluids, particle tracking could still occur even under conditions where the particles were blurred in the images. However, due to the low contrast, it was nearly impossible to tell where the cell boundaries lay, or whether objects were cells at all.

4.9 Fluorescent Imaging

In an effort to bypass the contrast limitation discussed above, a series of experiments were conducted using quail embryos for blood flow imaging. *In ovo* stage E 2.5 quail embryos were injected with Syto-11 nuclear staining dye (Molecular Probes) and mounted on an upright fluorescent microscope (Zeiss Axiophot). Staining the cells provided much better contrast between the blood cells and the surrounding tissue and media compared to the transmitted light images previously used. Several different high-sensitivity cameras were utilized for these experiments. The cameras were either mounted directly on the microscope or attached to an image intensifier. Due to either frame limitations or light sensitivity, the cameras were limited to slow acquisition speeds, so only slow moving extra-embryonic vessels were used. The flow velocity was further reduced since the eggs were imaged at room temperature, rather than the physiologic temperature of 37°C.

The i-PentaMax (Princeton Instruments) camera was extremely sensitive to light and was able to provide very clean images. The DPIV results were also of

good quality. However the frame rate of 15 Hz limited it to all but the slowest flows (Fig. 17).

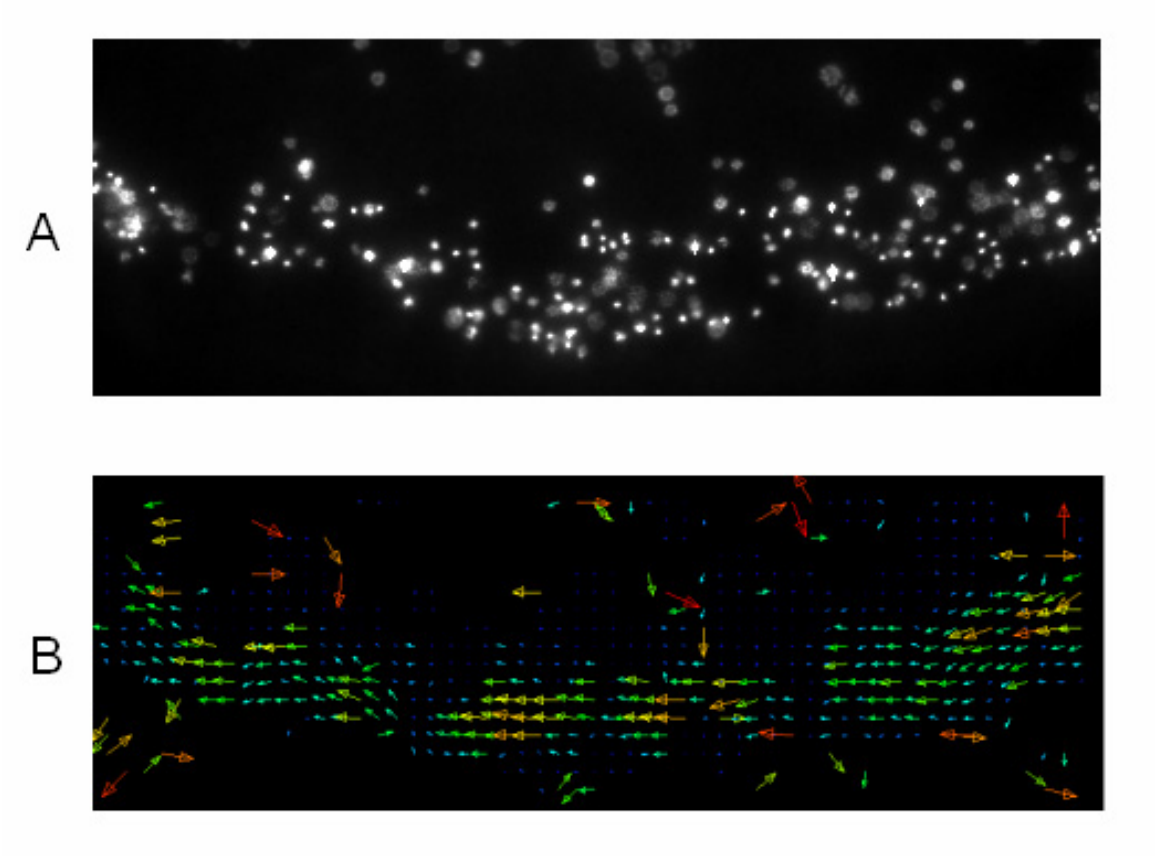

Figure 17: A) Image of labeled blood cells (white points) traveling through an extraembryonic vessel of quail embryo. B) Filtered DPIV results from image pair including the above image. Red vectors symbolize higher velocities.

A Phantom v4.2 (Visible Solutions) camera was also used for imaging. With an acquisition speed of up to 1000 fps, the phantom has the ability to image faster flows. However the camera was not as sensitive as the I-PentaMax and had to be used in conjunction with an image intensifier (Hammatsu). Due to the high levels of noise introduced by the image intensifier, the camera had to be kept at a low frame rate to keep the intensifier settings as low as possible. The

flow image and resultant DPIV reflect the higher noise levels with an increase in spurious velocity vectors (Fig. 18).

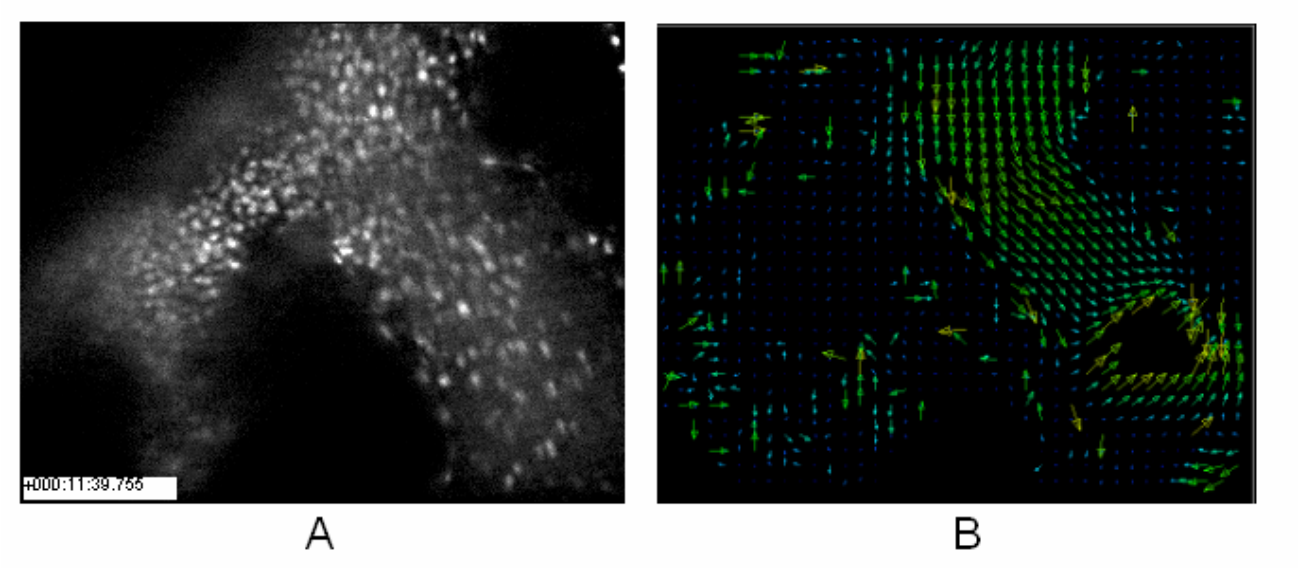

Figure 18: A) Image of flow inside an extraembryonic vessel in a quail embryo using the Phantom v 4.2 camera at 50 fps. Due to the use of an image intensifier there is a relatively high level of noise in the image. B) Filtered DPIV result of image pair including image A. Note the abundance of spurious vectors and the missing data in the right hand corner. This is believed to be caused by a thicker region of tissue partially obstructing the view into the vessel.

To summarize, the sensitivity and frame rate of exisiting cameras were not high enough at the same time. The sensitive cameras were too slow, and the fast ones not sensitive enough to produce images with a sufficiently high signal to noise ratio and close together in time. The use of an image intensifier (Hamamatsu) was tested, but the noise introduced to the images was too high. Despite the problems encountered, the use of fluorescent staining for DPIV analysis was able to capture the qualitative aspects of the flow, such as direction and general size of vessels (Fig. 19).

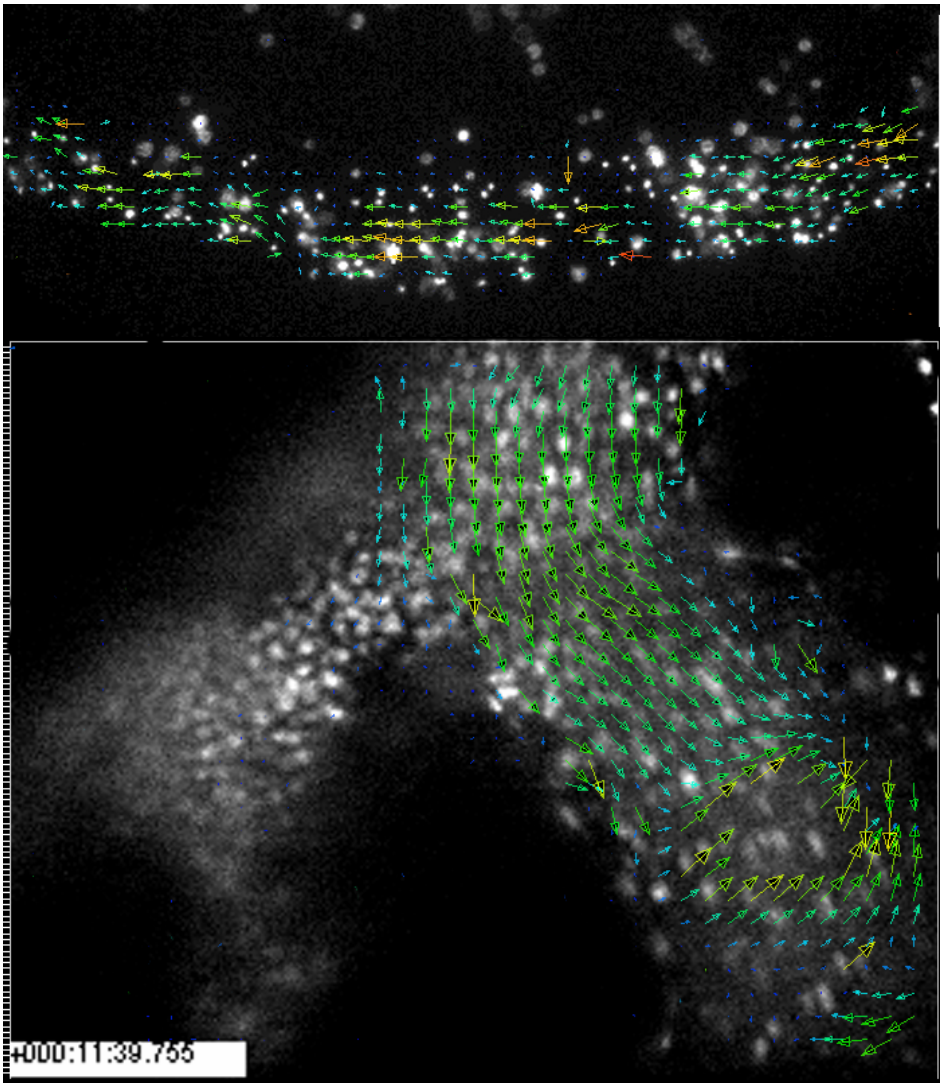

Figure 19: DPIV vectors overlayed with noise outliers removed for representational purposes. Along with the noise, the processing does seem to capture the essence of the flow.

DPIV analysis was performed on images acquired through a VIDIM microscope (20X objective, 1 sec between frames) of epsilon-globin::GFP transgenic mouse, which express GFP in their blood cells. Movement of blood through the blood-islets was recorded. At this stage, the lumens of the future

vessels are quite small, and only 1-2 cells can fit at a time through the channel. The results demonstrate the effects of large vessel size relative to the lumen. In the image below, there are many vessels crossing the screen, with about a 1 to 2 cell diameter width (Fig. 20A). In order to maintain enough cells within the interrogation region, the windows had to be large relative to the vessel widths. From the DPIV results (Fig. 20B), it can be seen that the necessary windows resulted in non-flow areas appearing to contain vectors. In other words, the area of flow is widened relative to the original image.

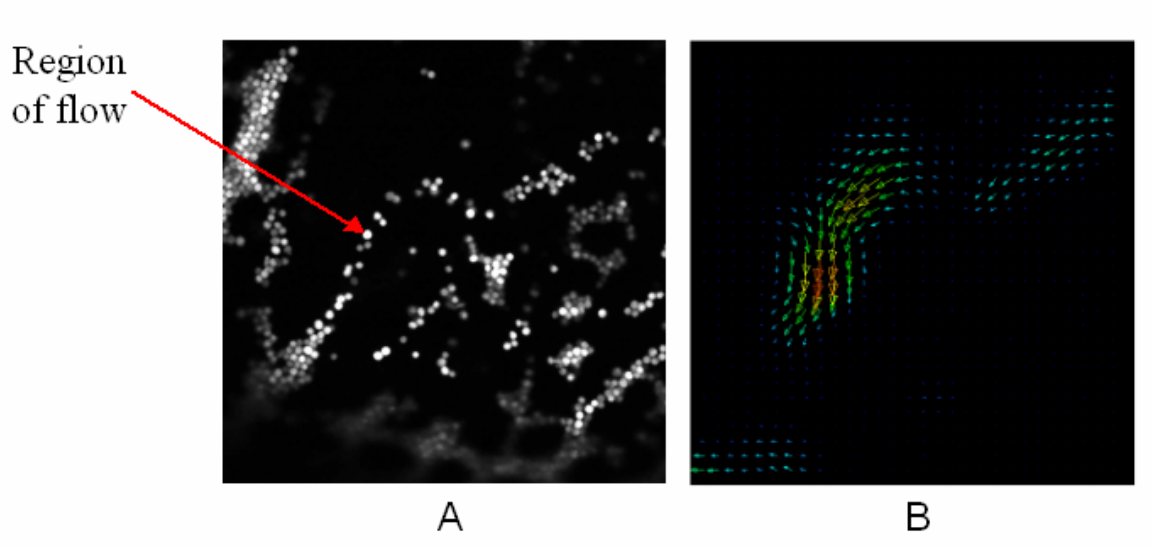

Figure 20: A) Original image of the blood islets (courtesy of Paul Kulesa). B) DPIV results, demonstrating widening of the flow region due to large window size.

4.10 New Fluorescent Techniques

Recent developments in high-speed fluorescent imaging have provided an exciting new route to *in vivo* DPIV. With advances in on-board chip gain for CCD

and CMOS cameras, the ability to have concurrent sensitivity and high frame rate has become reality.

For example, new work being done with a Zeiss 5-Live high-speed confocal microscope has acquired images at 175 fps of transgenic zebrafish (gata1::GFP) that express GFP in the blood cells. This frame rate may not be able to resolve the fastest flows in the heart, but in other vessels it has provided striking images. This new system allows to acquire fluorescent images at much higher frames, yet does not suffer noise issues encountered with earlier systems (Fig. 21).

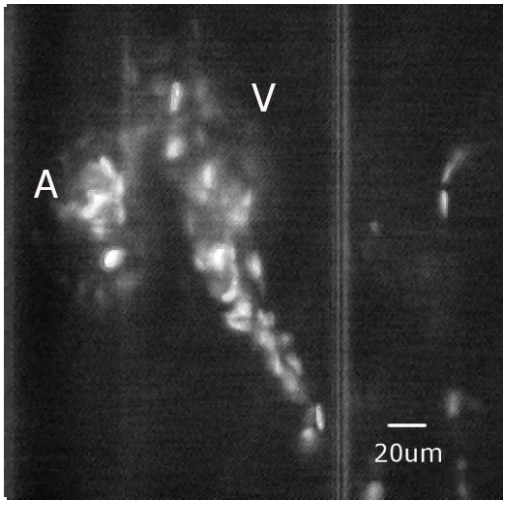

Figure 21: Image of flow inside embryonic gata1::gfp zebrafish heart acquired using Zeiss high-speed confocal microscope.

Chapter 5: Flow Modification

5.1 Introduction

The purpose of this work is to develop a method of altering blood flow *in vivo* in order to study the interplay of blood flow and vertebrate heart development. In this chapter the use of a implanted bead, then a magnetically induced bolus, to form obstructions in the blood flow are described.

As discussed in the first chapter, previous *in vivo* flow alteration experiments have focused on ligating, constricting, or ablating vessels in animals, a process that involves invasive surgery and possible side effects to the model. We seek to create flow alterations in embryonic zebrafish (*Danio rerio*) using novel and less invasive methods.

5.2 Bead Implantation

In the first experiment, 50 um glass beads were used to block blood flow in tie2::GFP transgenic embryonic zebrafish. These transgenics express GFP throughout the endocardium at early stages and then only in developed valves. Several 37 hpf embryo were anesthetized as previously described then mounted, ventral side up, on a 100 mm diameter petri dish in individual drops of low temperature melting agarose. After the agarose set, a small incision was made using a pulled glass micropipette tip, on the epithelium over the point where the two blood streams joined prior to entering the heart. Several beads were

sprinkled over the fish in an attempt to get some to end up on the fish near the incision. Using a tungsten needle, the bead closest to the incision was maneuvered over the incision and pushed down into the embryo. The fish were then returned to an incubator

Images were taken of the fish the following day at 57 hpf on the Zeiss Axiophot to note any changes in the position of the beads within the fish. In several cases the bead had come back out of the incision. Dish water was changed daily.

At 4.5 dpf, the fish were once again imaged to record the heart morphology as well as to note the position of the bead. Additional imaging was also performed on a confocal microscope (Zeiss 410) to check for the distribution of GFP, and thus to infer the state of valve development. There were 4 main bead positions observed: 1) the bead had left the fish, 2) the bead remained within the fish, but was not in the blood-inflow path, 3) the bead was lodged at the inflow to the heart, cutting off blood flow, and 4) the bead had entered the heart and was lodged at the outflow, cutting off all flow. The control fish were considered those in which the bead ended in a position near the heart, but did not affect the blood flow. Additionally, some fish had the beads removed an hour after implantation as a control of the implantation process itself. These fish demonstrated no effects from the procedure at 4.5 dpf.

Fish in which the flow of blood was blocked demonstrated three characteristic phenotypes. First, their hearts had greatly reduced outflow tracts (i.e., bulbus arteriosus), and the hearts did not loop. Additionally, the walls of the

inflow and outflow tracts collapsed and fused, beginning at 3 dpf. Furthermore, the second and third cases did not demonstrate valve development, as is shown by the lack of GFP localization in the confocal images (Figs. 22k, 22l).

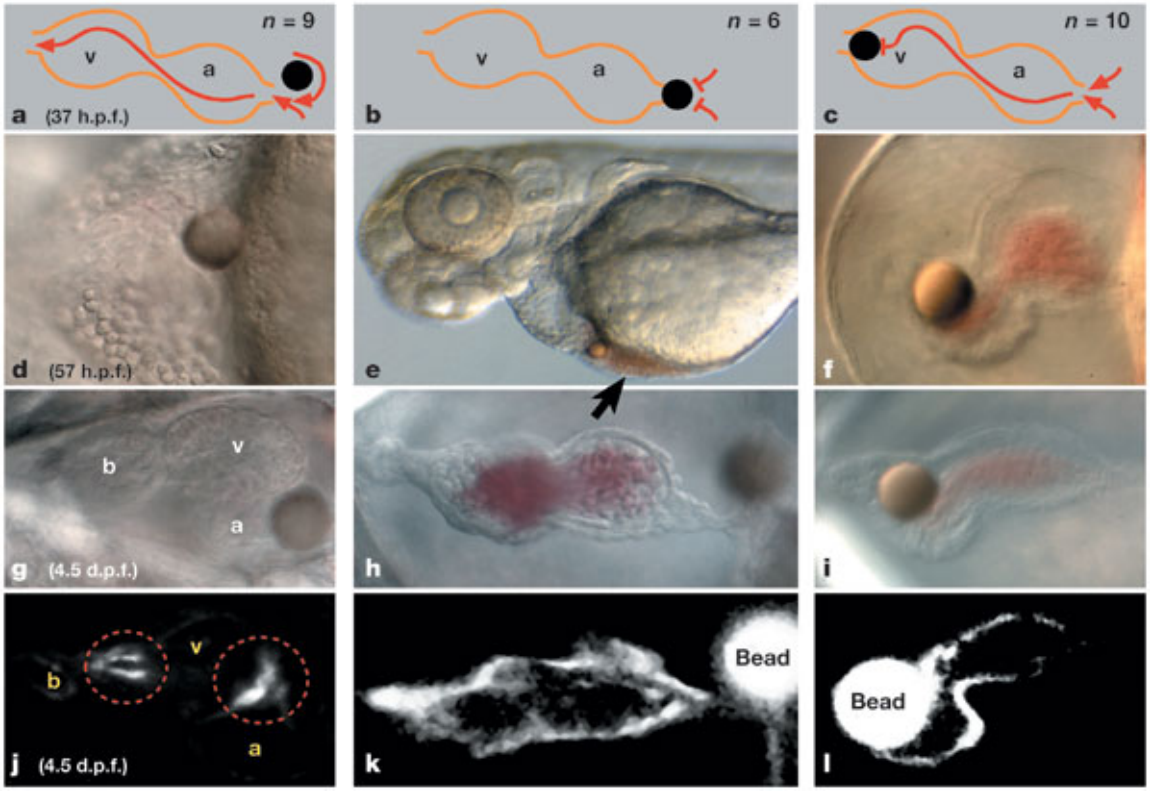

Figure 22: Comparison of embryonic hearts subject to bead implantation. First column shows little effects due to sole presence of bead when not blocking blood flow. The second and third columns show fusion of heart inflow and outflow, and lack of valve development as shown by the fluorescent images (22k and 22j). (*From Nature 421: 172-177***)**

The similarity of the defects resulting from disrupting either inflow or outflow suggests that it is not the changes in cardiovascular transmural pressure that is responsible for the observed effects, as the two different blockages should decrease (blocked inflow) or increase (blocked outflow) the pressure. Lack of oxygen or nutrients is not likely to be a factor in the results either based on

experiments by Pelster and Burggren (1996), which showed that embryonic zebrafish do not depend on hemoglobin for oxygen transport during the first 7 days post fertilization, and that due to their small size and low metabolism they can obtain oxygen and nutrients through diffusion. The lack of effects to the heart in the bead removal controls as well as the fish with implanted non-affecting beads indicates that the implantation process is not responsible for the observed effects either. Instead, the decreased shear force, the common feature of these treatments, seems most likely to generate the developmental phenotype. These studies make a strong case that blood flow is a necessary factor for functional heart development in vertebrates.

Although this technique is effective, there are several areas for improvement. The primary drawback with the bead occlusion method is that the final location of the beads is a matter of chance. The three final bead positions discussed in the paper: blocking inflow, blocking outflow, and outside the direct path of blood to the heart, are not controlled during the surgical procedure. As such, one cannot choose *a priori* where to place the beads. This makes the method unsuitable for creating flow disturbances at specific points in the vasculature.

A third drawback of the bead occlusion method is that it only creates a binary (on or off) flow blockage. Due to the bead position being a matter of chance, it is not possible to devise an experiment that blocks the flow for only a certain amount of time or at a specific developmental stage. Additionally the beads cannot be made to partially obstruct the flow (e.g., to create a 50%

blockage of the blood flow into the heart). Our magnetic technique presented in the next section not only allows one to pinpoint the location of the flow blockage or disturbance, but also allows one to decide when and how long to leave the blockage in place.

In the process of conducting our flow experiments, we discovered an unexpected side-effect that may reduce the compliance of the heart wall itself, a potentially useful means of mimicking certain cardiac pathologies that result in reduced cardiac performance.

5.3 Magnetic Flow Control

A magnetic flow control technique was chosen as an alternative means of creating a site-specific, reversible flow alteration. The work of Hayes *et al.* (2001) demonstrated the effects of a suspension of magnetic particles in small diameter tubing, providing the basis of our approach. In Hayes' work, a suspension of paramagnetic particles was loaded into a thin (80 um ID) capillary tube. When a *rare-earth* magnet was brought into the proximity of the capillary tubing, the particles aligned themselves in thin columns parallel to the magnetic field lines. Moving the magnet relative to the tube caused the columns of particles to adjust their position in order to remain parallel to the field lines. To test the potential utility of this procedure we reproduced these experiments (Fig. 23).

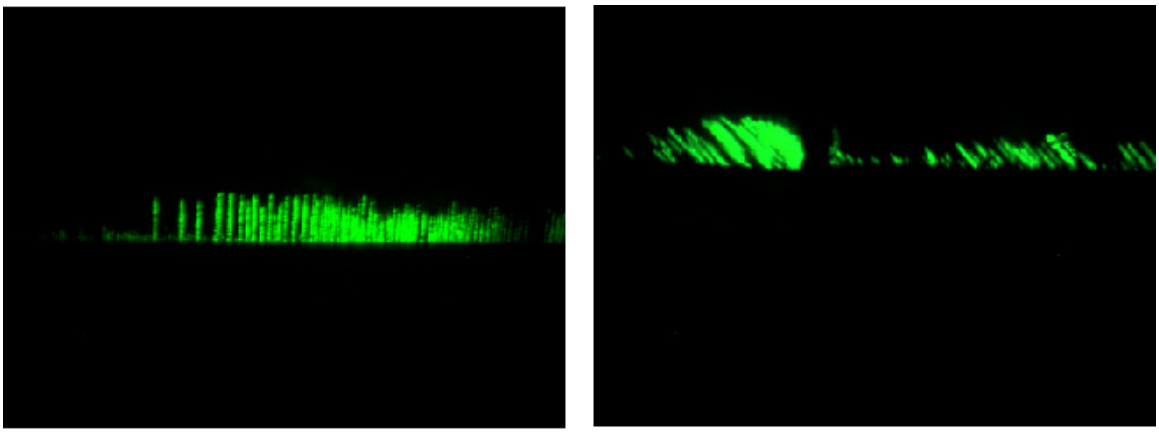

Figure 23: Magnetic particles orient themselves according to the position of a rare earth magnet. The magnet is directly below the green particles in the picture on the left, and offset by 50 degrees on the right.

We chose to use a miniature electromagnet developed by Dr. Barbic of Caltech in conjunction with the paramagnetic particles rather than following the design of Hayes because the rare-earth magnets used in his experiments were the same size as the embryo, therefore making the possibility of localizing the magnetic particles to a specific site within the embryo unlikely. Depending on the voltage passed through it, the magnet was capable of producing forces of at least 10 pN. Our primary hypothesis was that a slurry of particles, introduced into the embryonic circulation, could be precisely placed at a desired location within the zebrafish vasculature by attraction to the field lines of a properly positioned micro-electromagnet. The rotation of the field lines, and hence the particles, was to act as an on-off valve for the flow. The result of such an accumulation of particles would be a disruption in the normal blood flow patterns. To find the optimal parameters for using this technique *in vivo,* different materials and experimental conditions were evaluated. Magnetic particles, fish orientation, and field strength were all considered appropriate variables to be tested.

5.4 Preliminary Baseline (*In Vitro*)

We first conducted *in vitro* experiments to test the effectiveness of the magnet with our paramagnetic particles. Although rare-earth magnets had been shown to work, the ability of the electromagnet to form either columns of particles or a bolus was not known. A Beckmann micro-loader tip was filled with a 1:4 dilution of stock 2.5% solids suspension of 1-2 um Polystyrene Superparamagnetic Microspheres (Polysciences Inc.) in water, and then placed underneath a microscope. Based on Barbic's work, a wall thickness of approximately 40 um is desirable for the magnetic forces to be strong enough to move the particles under static flow conditions. Our magnet was positioned manually using a micromanipulator (M3301, World Precision Instruments) and was powered by a regulated current source. We observed that when the magnet tip approached the tube, the particles, instead of forming parallel columns, formed a bolus at the point nearest the magnet tip and could be readily moved within the tube (Fig. 24). While these experiments demonstrated that the electromagnet could attract a large group of particles at scales similar to that encountered in the fish, the resultant shape was quite different compared to the rare-earth magnet. Despite the inability to create "valves" using the particles, the presence of a bolus could be enough to alter blood flow. The ability of the magnet to manipulate the particles even through a plastic barrier suggested that the thinner barriers between the blood stream of the fish would not pose a problem for our experiments.

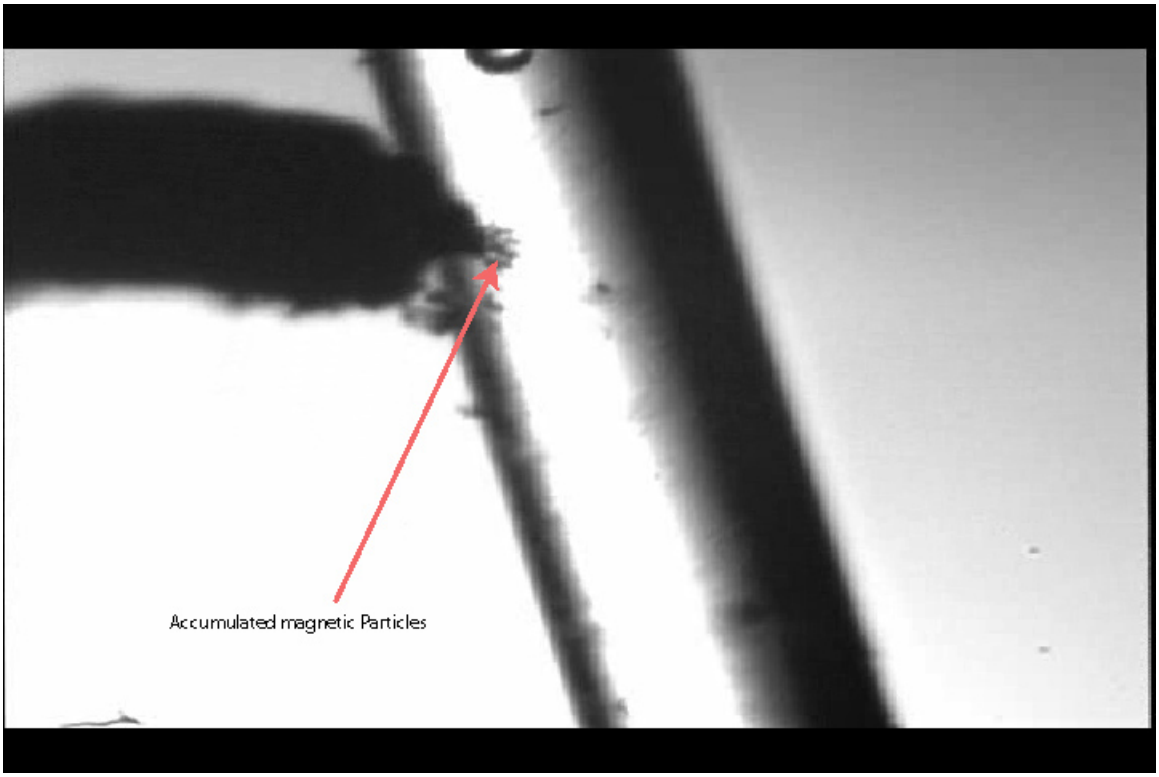

Figure 24: The miniature electro-magnet is able to collect magnetic particles inside of a microloader tip.

5.5 Preliminary *In Vivo* Static Experiments

Two different types of magnetic particles were tested for these experiments. 1 um paramagnetic particles (iron oxide embedded in polystyrene) and 250 nm (nanomag-D-greenF –PEG 300; Micromod, Germany) were examined. The first *in vivo* tests involved injecting the 1 um sized particles directly into the yolk sac of a 48 hpf embryo to examine if the magnet would be strong enough to localize the dispersed particles through a viscous medium such as the yolk sac. The magnet was placed against the epithelium, and the movement of the particles was tracked. Figure 25 shows the movement of the

particles over the course of approximately 175 minutes. Particles first reached the magnet's location at 62 minutes after the magnet was positioned against the fish.

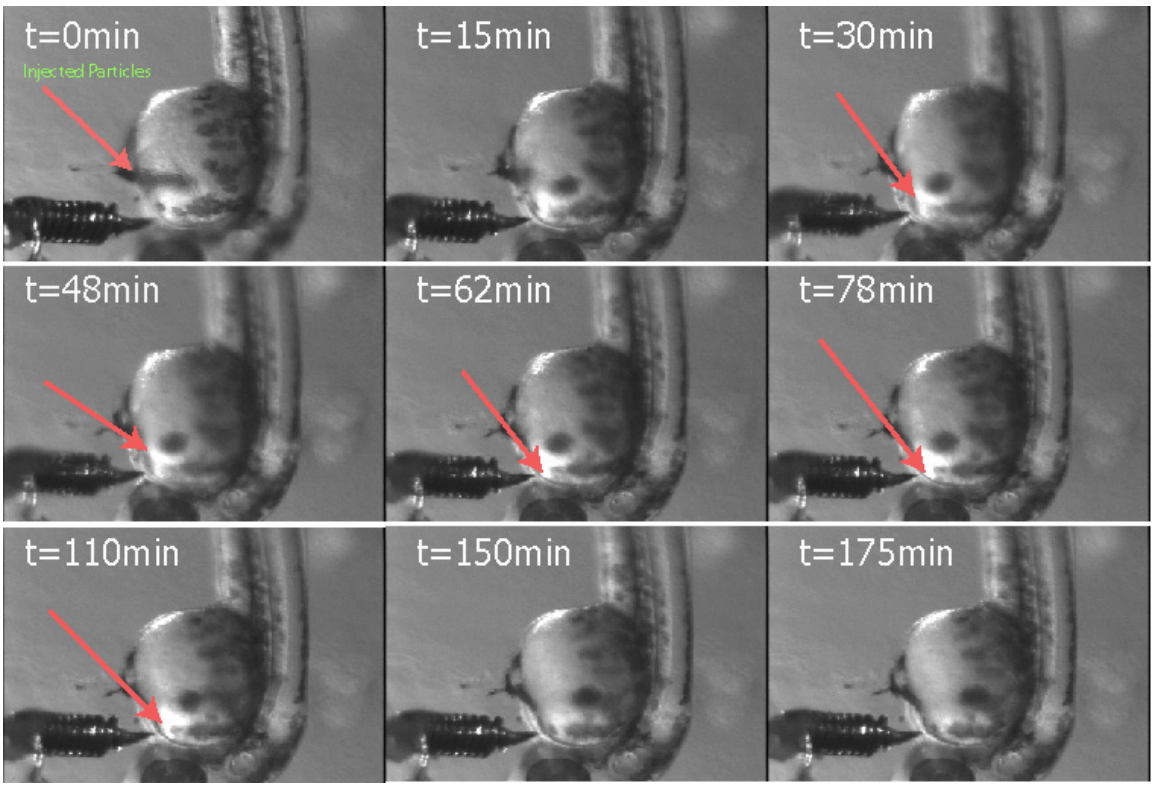

Figure 25: Time sequence of particles moving toward magnet in embryonic zebrafish. The particles start on the edge of the yolk sac on the left side of the fish and slowly migrate towards the anterior end of the fish.

The 250 nm magnetic was next tested for response in the yolk sac of a 48 hpf fish. It was noted that overall ease of injection with a 15 um micropipette tip opening was greater with the smaller particles due to less micropipette clogging. As before, the magnet was brought near the bolus of magnetic particles, and the time necessary to position the bolus was recorded. The undiluted suspension of particles formed a bolus near the point of contact between the fish and the

magnet (Fig. 26). It was observed that the smaller particles had a more rapid response time to the magnet than the 1 um particles: 15 minutes as compared to 62 minutes for the larger particles.

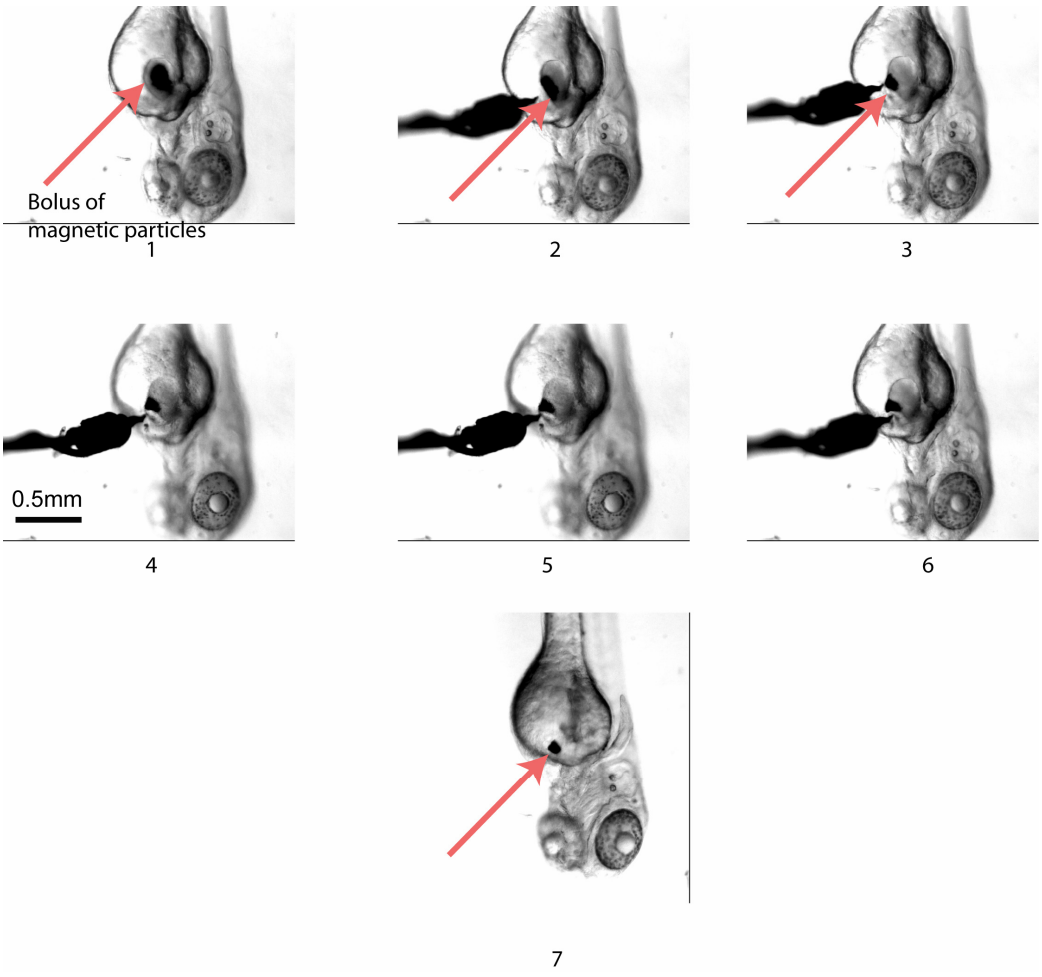

Figure 26: Movement of 250 nm particles injected into the yolk sac after application of the magnet. Notice the difference between the initial dispersion area and the final compact bolus.

Based on the more rapid response time and ease of injection, the 250 nm particles were chosen for the rest of our experiments.

To test the behavior of the particles in a more dynamic environment than the yolk sac, the magnetic particles were injected into the fish at the point of confluence between the two veins returning flow to the heart. The particles did not enter the blood stream, but ended up in the pericardial sac surrounding the heart. The particles responded immediately to the placement of the magnet near the heart, even though the moving heart walls were adjacent to the particles, and most particles had formed a bolus around the magnet in 45 minutes (Fig. 27). The magnet was removed after 14 hours. The particle clump began to disperse immediately upon removal of the magnet, and upon inspection 2 days later the bolus of magnetic particles had dispersed from the cardiac region. Based upon these observations, it was determined that the particles would remain in position even when exposed to forces caused by wall motion under the presence of the magnetic field, and yet would also disperse afterwards.

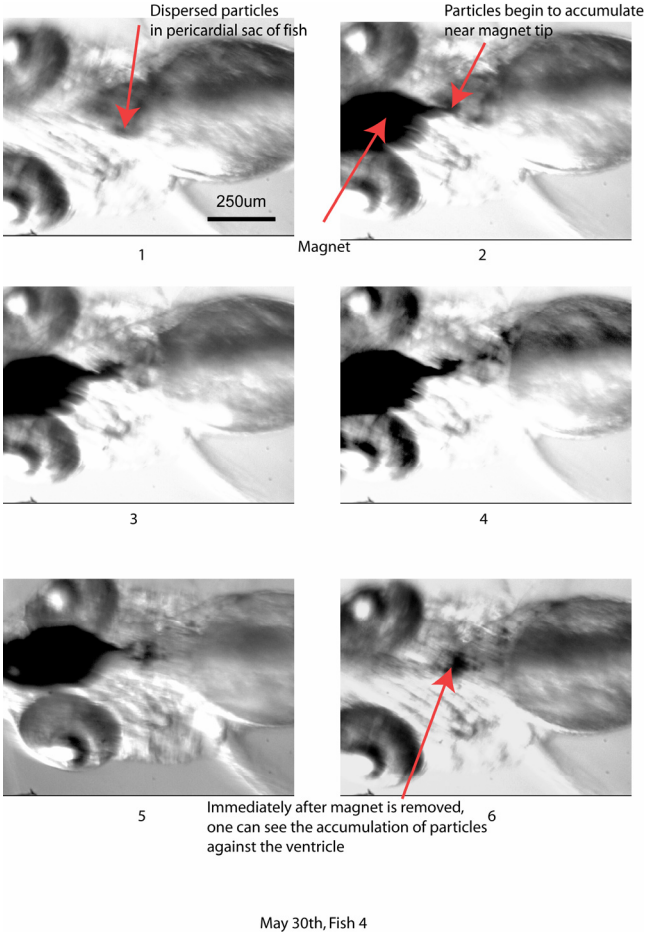

Figure 27: Collection and movement of magnetic particles in the pericardial sac of the embryo.

5.6 *In Vivo* Flow Alteration

Practice and smaller micropipette tip diameter allowed for more precise positioning of the injection site. Two different sets of flow blockage experiments were performed on 48 hpf embryos. Flow blockages were created in a caudal region of the dorsal aorta (DA) and at the sinus venosus.

To test whether the magnet would be able to form a bolus of particles in a dynamic flow environment subject to fluid drag, using the injection techniques

mentioned in the methods chapter, a small volume of particles was injected into a caudal region of the DA in a 48 hpf embryo. This region was chosen as the injection site for its superior optical and surgical accessibility. Additionally, the distance of the injection site to the heart minimized potential injection-related trauma to the heart itself. The intravascular-injection introduced particles into the bloodstream as well as depositing some in the surrounding tissues (e.g., Fig. 28). The fish were transferred from the injection room to a separate magnet workstation within 5 minutes after the injection procedure was complete. Microscopic observation revealed that the injection itself had obstructed blood flow to the lower tail (Fig. 28), and that there was no circulation in the fish although the heart was still beating.

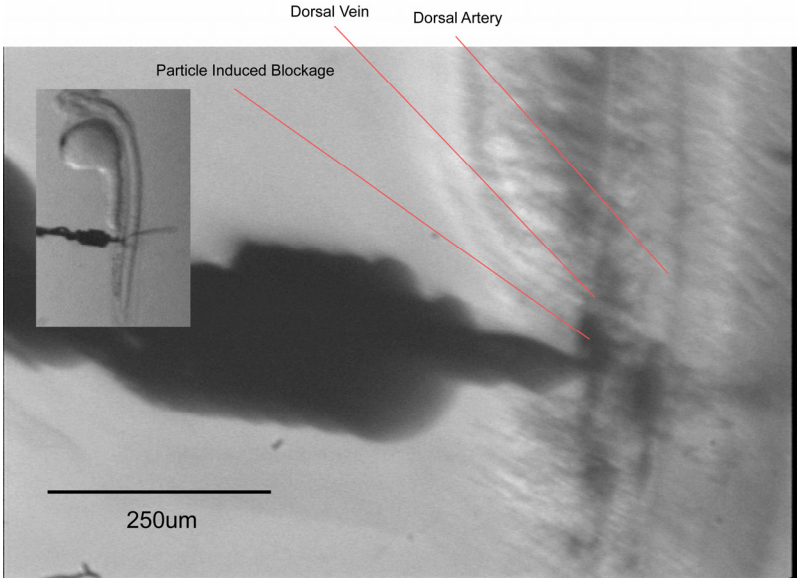

Figure 28: The magnet was placed near the blockage in the tail and was able to prevent blood flow from reaching the lower tail.

One hour after particle injection the blood flow in the caudal region of the tail spontaneously restarted with small clumps of magnetic particles traveling with

the blood. The magnet was applied to the fish at a voltage of 50V and positioned near the original injection site; one of the circulating clumps was captured. Careful manipulation of the magnet resulted in repositioning of the bolus near a bend in the vessel, again stopping blood flow. Approximately 75 minutes later we observed that while the flow to the caudal region remained obstructed, blood was being shunted from the DA to the dorsal vein (DV) via an intersegmental vessel and was thus able to return to the heart. The magnet was removed from the fish after 10 hours, and consequently the bolus dispersed, resulting in flow being restored to the lower tail and throughout the fish.

High-speed imaging of the heart revealed numerous changes in the test fish including lower average systolic blood velocity through the V-B valve (2.1 mm/s) than was recorded for control fish (3.3 mm/s). To estimate contractile fraction, the major and minor axes of the heart during end diastole and end systole (denoted with a subscript 1) were measured and their ratios compared. The test fish (n=1) showed a larger contraction a_1/a= 0.6 and b_1/b = .5 while the control fish (n=1) had fractions of a_1/a= .8 and b_1/b= 0.8. The discrepancy in contractile fraction in this case may be attributed to the slightly different viewpoint obtained while imaging.

5.7 Cardiac Flow Alteration Experiments

We observed that after the intravascular injections, the particles accumulated and then settled out just before the inflow to the heart, directly above and to the side of the yolk sac (e.g., Fig. 30). Although the settling out of the particles was expected due to a density greater than water, the location was a surprise. This unexpected result was advantageous as it wasn't necessary to perform the injection near the heart itself; instead the particles still could be injected in the tail and then collected over the yolk sac after they had settled out of the mainstream flow. Two sets of experiments were conducted to alter the blood flow into the heart. Embryos were injected at 50 hpf with two different magnet orientations used to form a bolus and block blood flow. Blood flow velocity, heart beat frequency, and contractile fraction were measured at 4.5 dpf to determine the effects of the treatments on the system.

5.7.1 *Side Mounting*

A 50 hpf embryo was injected with particles in the DA. Leaving the fish on its side, the magnet at full voltage was placed near the yolk sac to capture the deposited magnetic particles. The gathered particles formed a bolus near the magnet tip after several minutes of exposure to the magnetic field. By changing the position of the magnet and the bolus over the course of 9 hours, the inflow to the heart was ultimately blocked. During the period of flow stoppage the red blood cells pooled on the side of the yolk sac, upstream from the blockage.

The fish was left overnight, and upon returning 11 hours later, the particles had formed small unresponsive boluses, and the flow had resumed. Dynamic response of the heart to treatments at 4 dpf could not be examined due to fish death.

Another side-mounted fish was prepared for testing. The particles responded immediately to the presence of the magnet, and the flow was blocked within 2 hours. The fish and magnet position were monitored every 2 hours for 6 hours. The magnet was maintained at full power, and its position was adjusted when necessary to maintain the flow blockage. The next morning flow had restarted, and just as in the previous case, the bolus of particles had broken into smaller and unresponsive individual boluses. Upon closer examination it appeared that the particles had been pulled through the tissues surrounding the heart. Observation two days later showed an abnormal heart shape, lower velocity, edema, and strong regurgitation (Fig. 29).

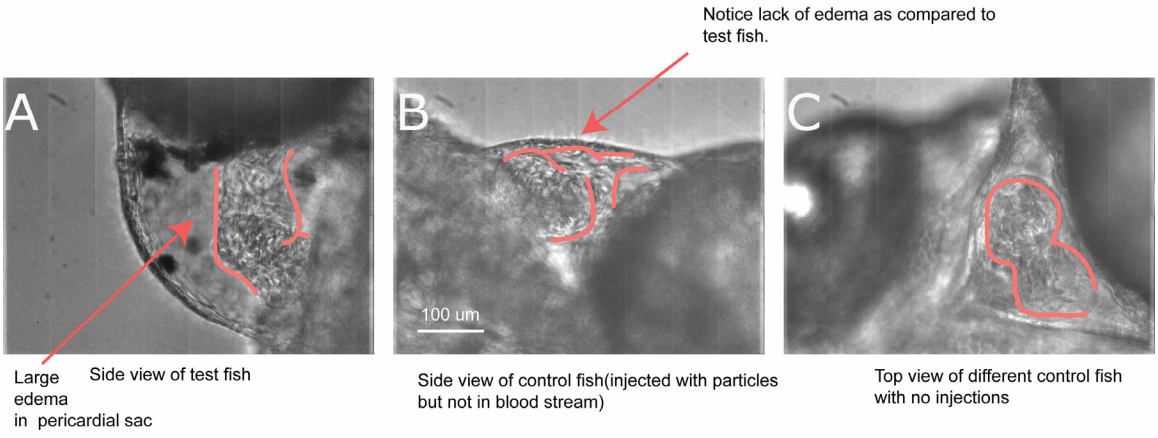

Figure 29: The fish in (A) had its blood flow blocked with the magnetic particles. Notice the edema and undeveloped heart. (B) and (C) show the control fish hearts. (B) shows the heart from the side, highlighting the normal pericardial shape.

The test fish's (n=1) average peak systolic velocity through the V-B valve was calculated to be 2.2 mm/s while the average velocity for two control fish was 4.3 mm/s (Standard deviation, σ, =0.27). The test fish showed a depressed contractile fraction with an a_1/a of 0.7 and b_1/b of 0.9 compared to a_1/a and b_1/b measurements of 0.6, 0.7 and 0.5, 0.4, respectively, for the two control fish. Neither of the control fish hearts demonstrated edema or regurgitance.

5.7.2 *Dorsal Mounting*

A third fish was oriented yolk sac upwards instead of on its side after injection. The improved view of the cardiac area allowed for better positioning of the magnet and bolus. The blood flow was blocked within one half hour (Fig. 30), compared to a minimum of 2 hours using the side-mounted orientation.

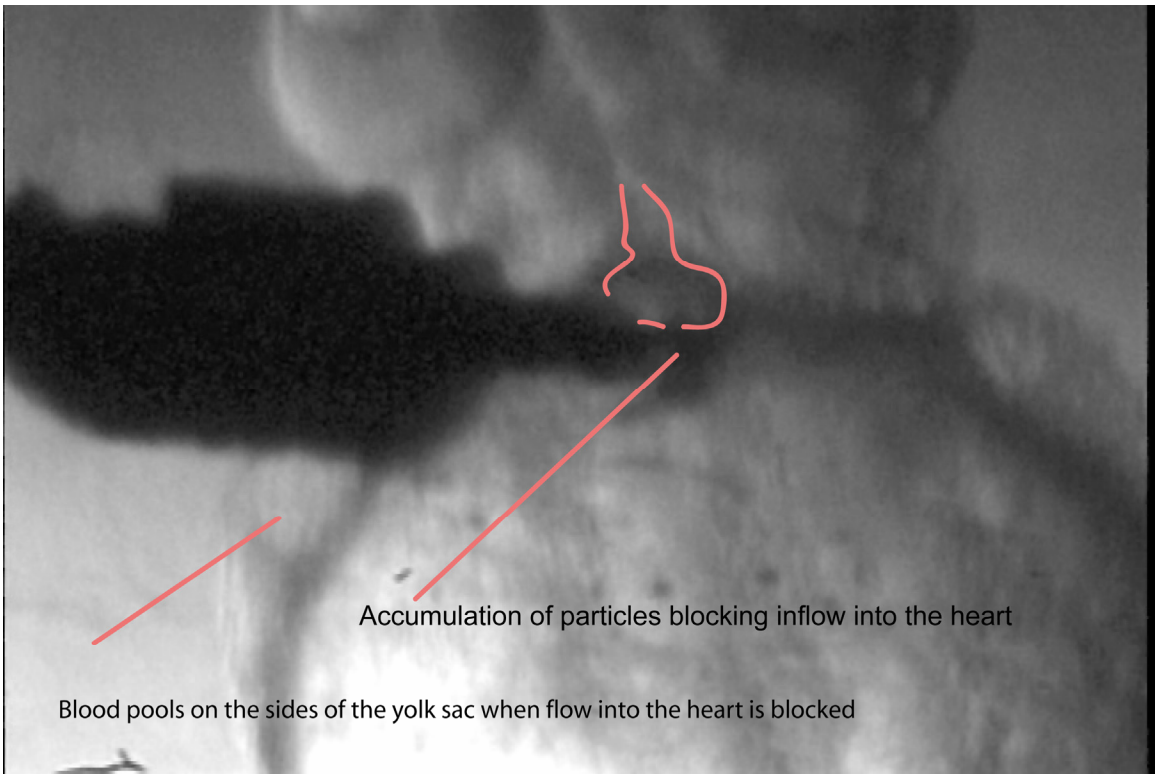

Figure 30: The bolus of particles sits at the entrance to the heart blocking the flow and blood pools on the side of the yolk sac.

In an attempt to prevent the particles from being drawn into the tissue surrounding the blood vessels, the voltage was lowered from the maximum of 50 V to approximately 25 V after the bolus was formed. This seemed to delay the absorption of the particles into the surrounding tissues to 17 hours. Observation at 4.5 dpf showed that the test fish had a slower systolic flow, 3.9 mm/s, compared to 8.8 mm/s and 5.6 mm/s for control fish 1 and 2 (Fig. 31). The heart contractions were noticeably weaker with an a_1/a and b_1/b of 0.99 and 0.6 while the control fish had measurements of 0.7 and 0.4 for the same ratios. The heart

itself was more elongated than the control hearts, although the valves were present and functioning.

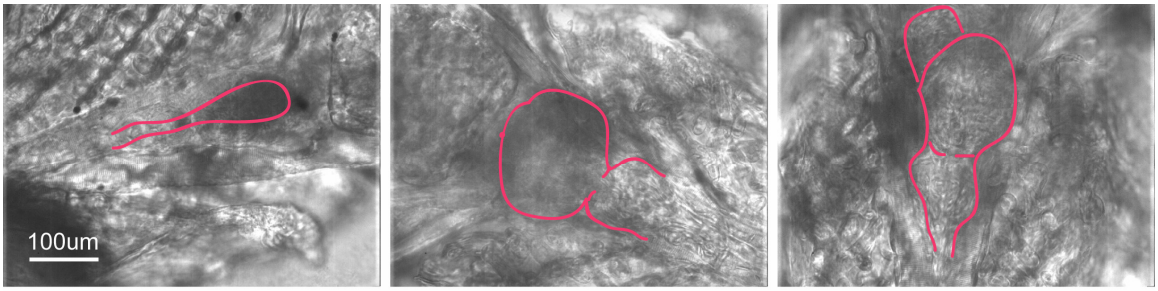

Figure 31: Test case 3, fish on the left, had underdeveloped and poorly performing heart as compared to the controls (1, 2).

5.8 Control Experiments

To test that the presence of a local electromagnetic field or the particles by themselves did not have any deleterious effects on the fish that could be responsible for the observed changes in the heart morphology, a series of control studies were carried out. The first focused on the effect of the particles in the blood stream with no applied magnetic field, the second on the effects of the magnetic field itself.

For the first set, particles were injected into the blood stream of three embryos at 50 hpf. In addition, one fish was not injected but was exposed to a magnetic field for 19 hours, and three fish were mounted but were not subjected to either injections or magnetic field exposure. The intracardiac blood flow and heart morphology of the fish were observed at 4.5 dpf. Visual inspection

revealed no obvious morphological differences caused by the injection of the particles (Fig. 32 and Table 1), although one control fish did develop edema.

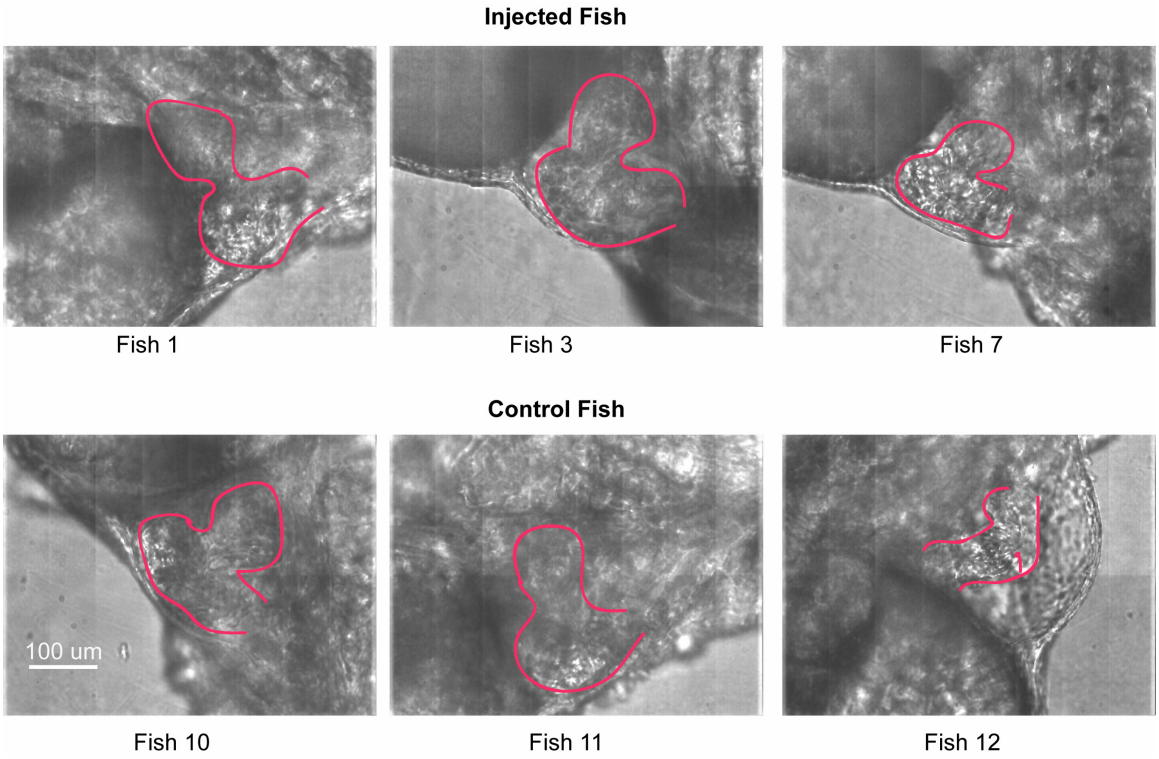

Figure 32: Hearts at 4.5 dpf. The top three fish were injected with magnetic particles, while the three fish on the bottom had nothing done to them. All fish developed multichambered hearts, although fish 12 displayed edema.

Table 1: Measurements for injection and magnetic controls at 4.5 dpf.

Fish	type	Vel(mm/sec)	a_1/a	b_1/b	bpm	edema	regurgitance	valves present
1	inject	2.8	0.49	0.52	123	N	N	Y
3	inject	2.8	0.47	0.5	135	N	N	Y
7	inject	2.8	0.47	0.53	115	N	N	Y
9	magnet only	1.8	0.93	0.71	115	Y	Y (V-B)	N
10	control	2.6	0.53	0.57	129	N	N	Y
11	control	2.5	0.45	0.43	137	N	N	Y
12	control	2.4	0.55	0.32	151	Y	N	Y
σ(treating fish 9 as an outlier)		.18	.04	.09	12.4			

The magnetic test fish, fish 9, developed a non-looped heart with severe edema and regurgitance (Table 1 and Fig. 33).

Additionally, it exhibited a slower velocity than both the injected and control fish, 1.8 mm/s as compared to an average of 2.8mm/s for the injected fish and 2.5 mm/s for the control fish. Furthermore this heart contracted much less than both the control and injected fish and had a lower heart rate than the averages for both groups (Table 1).

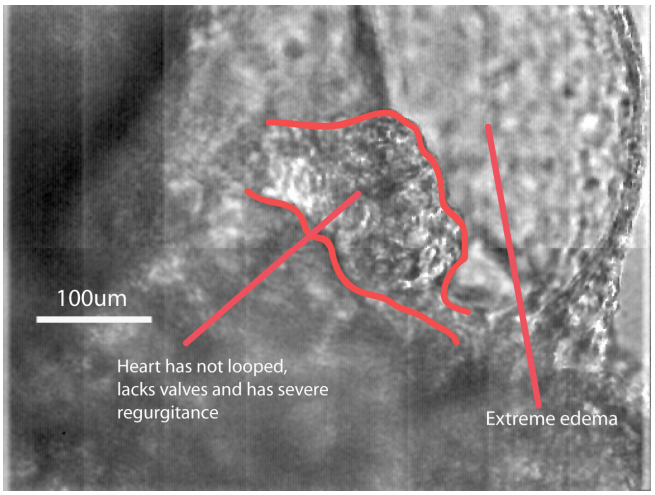

Figure 33: Magnet-only control fish heart at 4.5 dpf. Note the lack of looping, small size, and large edema.

A possible explanation for the defects in fish 9 could be compression by the agarose. In the course of positioning the magnet for these experiments, it was observed that in pushing the magnet towards the fish, the agarose was pushed in and often compressed the vessels leading into the heart, thereby reducing blood flow.

The experiment was repeated with five fish. Fish number 5 was exposed to the magnetic field for 12 hours at approximately 35 V, and the other four fish served as controls. This time, some of the agarose near the heart of the fish was removed in an attempt to not impact the heart by pushing the agarose against it during placement of the magnet. The five fish were collected and observed under the high-speed camera at 4.5 dpf. All five fish had looped hearts as expected for that developmental stage (Fig. 34 and Table 2).

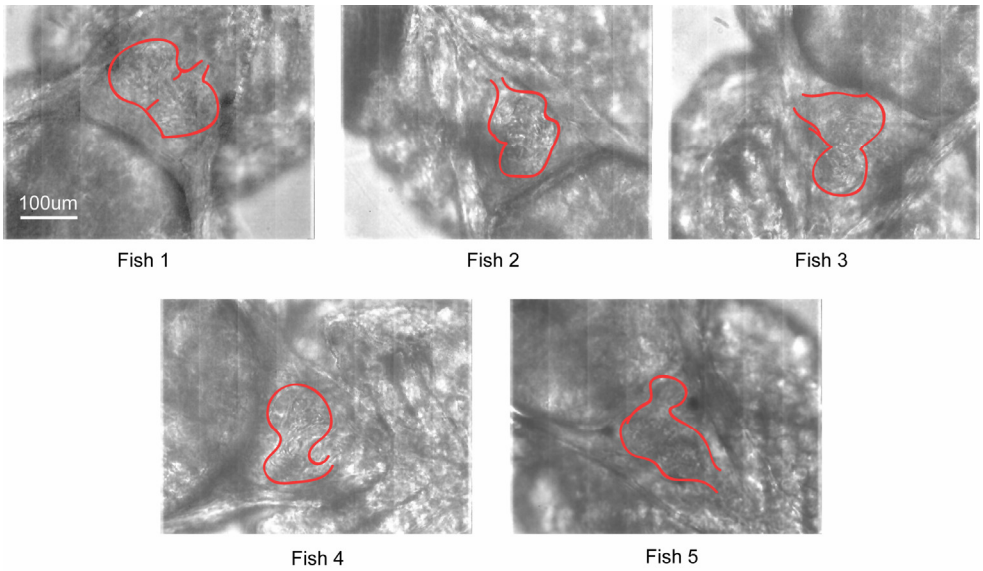

Figure 34: Test (Fish 5) and controls for magnetic effects at 4.5 dpf.

Table 2: Measurements for magnetic field controls at 4.5 dpf.

fish	Vel(mm/sec)	a_1/a	b_1/b	bpm	edema	regurgitance	valves
1	3.02	.55	0.41	181	N	N	Y
2	3.75	.66	0.28	145	N	N	Y
3	6.28	0.51	0.25	170	N	N	Y
4	3.8	0.62	0.67	164	N	N	Y
5(test fish)	2.5	0.52	0.38	142	N	N	Y
σ	1.5	.07	.17	16.6			

The experiment was repeated again with four 48 hpf fish. One was exposed to the magnetic field for 10 hours. Unfortunately, the fish floated free from the agarose during the night, so individual identification was not possible.

Regardless, the fish were imaged at 4.5 dpf to compare their hearts (Table 3 and Fig. 35). All were found to have looped and to possess valves. Two fish had slight regurgitance back into the atrium at the end of diastole.

Table 3: Measurements from second magnetic field control set.

fish	Vel(mm/sec)	a_1/a	b_1/b	bpm	edema	regurgitance	valves
1	4.0	0.35	0.38	131	N	N	Y
2	4.1	0.51	0.51	115	N	slight(atrium)	Y
3	3.8	0.61	0.68	131	N	slight(atrium)	Y
4	4.2	0.64	0.54	131	N	N	Y
σ	.17	.13	.12	8			

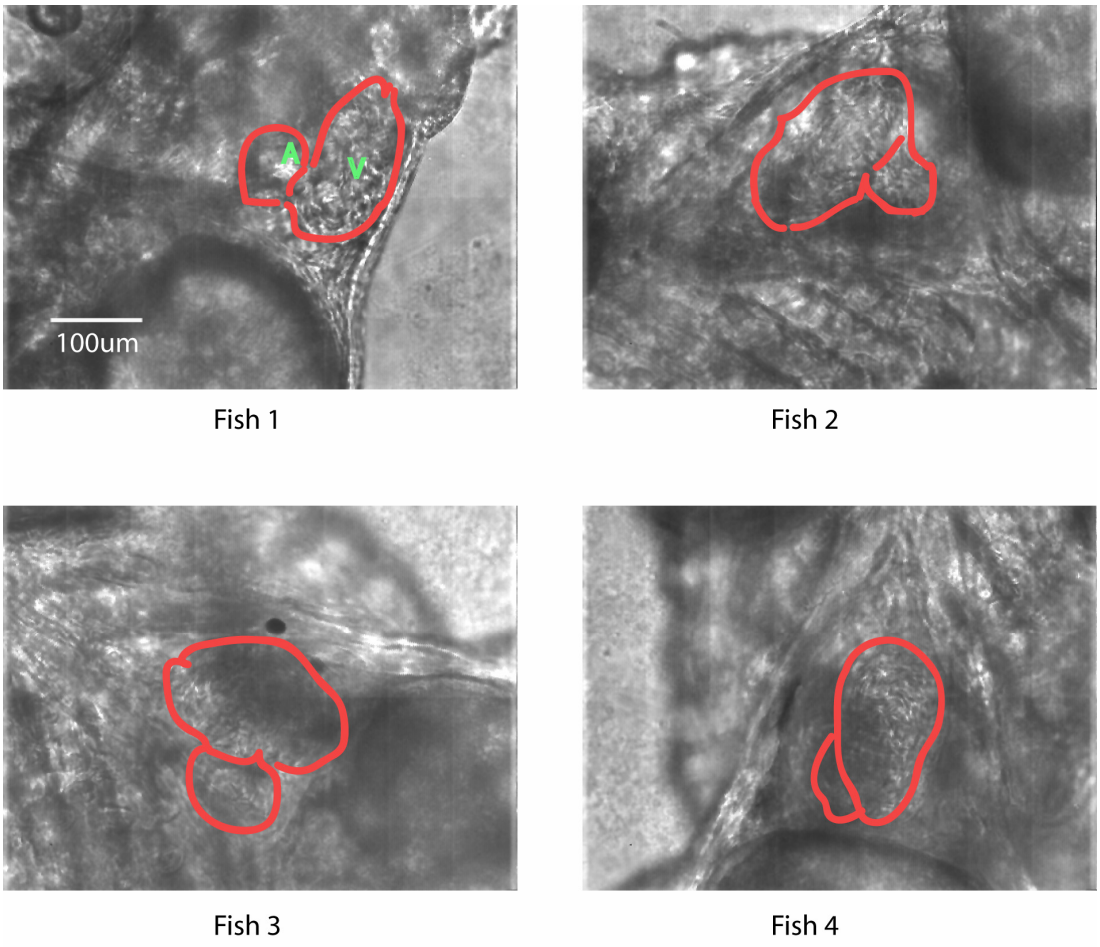

Figure 35: A comparison between the 4.5 dpf hearts of the last control set.

From Table 3, we can see that the velocities were within 10% of each other and none of the fish suffered from edema or regurgitance. There was some variation in the contractility, but not as much as in previous cases. Fish 2 had a slower heart rate, but the velocity and contractility were not markedly different from the other fish. The fact that one fish does not express an extremely altered morphology is a promising indicator that the magnet does not necessarily impact the fish.

Chapter 6: Conclusions

The objectives of this study were to apply a novel technique to the problem of mapping internal blood flow during development, develop a technique for delivering and positioning small magnetic particles into the developing circulatory system, and determining the effects of occluded and restarted flow on the major events of cardiogenesis. Several sets of experiments were carried out in an attempt to accomplish these goals. In the first set, a high-speed CCD camera mounted on a compound microscope was used to obtain images of the intracardiac flow environment in an embryonic zebrafish (*Danio rerio*). These images were then processed using DPIV. This demonstrated the first instance of *in vivo* intracardiac microscale DPIV, which in conjunction with particle tracking, produced quantitative flow data.

The second set of experiments created a novel technique combining sub-micron particles and a micro-electromagnet to create localized and reversible *in vivo* flow alteration in embryonic zebrafish. The particles were injected into the blood stream of the fish, and the magnet was used to localize the particles into a moveable bolus. The effects of altered flow were compared against control fish and expected stage-specific heart morphology. The zebrafish was chosen as our model due to its numerous advantages in imaging and handling over other vertebrate models, and the specific stage was chosen to allow easy comparison with non-injected fish. The results from both sets of experiments are presented

below. Using both of the first two objectives, the effects of flow on cardiogenesis were examined.

First, the intracardiac flow in embryonic zebrafish is highly dynamic. The results from DPIV showed the presence of jet in both the ventricle and bulbus arteriosus during diastole and systole, respectively. Additionally, regions of vorticity were observed on either side of these jets, along with extremely high levels of wall shear stress near the constriction or valve regions.

Secondly, altering the flow in early stages of zebrafish development resulted in abnormal heart development. Fish subject to flow blockage using the technique developed in this project generally demonstrated hearts with weaker contractions, slower heart beats, and lower flow rates. Additionally, increased levels of cardiac edema and blood regurgitation as well as less developed valves were observed. Based on the results of these experiments several conclusions can be drawn.

The first conclusion to be drawn is that DPIV has the potential to become an important tool for mapping the internal flows. Due to the large size of the cells relative to the vasculature and to lack of contrast between the cells and surrounding tissues, as used in the project, DPIV alone cannot quantitatively be used to describe the flow field. Overall flow patterns can be obtained from DPIV, but in this study manual particle tracking was needed to extract velocity information.

New developments in high-speed confocal microscopy may also help in improving the quality of *in vivo* DPIV data. As mentioned, it was necessary to use

a combination of DPIV and particle tracking to extract blood velocity from the images. With improvements in high-speed confocal microscopy and CCD motion cameras, it is now easier to acquire images at rates greater than 30 fps (Coates *et al.,* 2004; Nakano, 2002). Zebrafish lines that express GFP on the blood cells (Long *et al.,* 1997) could prove useful for particle tracking methods, or small fluorescent particles could be injected into the blood and used as tracer particles to provide a more ideal DPIV data set. Care would need to be taken to ensure that the particles were small enough and of proper density to accurately follow the blood flow, and that they had a sufficient concentration for DPIV yet did not disturb the cardiac function of the fish. The ability to extract more accurate quantitative data will be extremely important in linking altered blood flow and its effect on the heart.

Improvements in software may also aid in utilizing DPIV for *in vivo* flow studies. Due to the large size of the particles relative to the vasculature, an automated approach using particle tracking to guide the DPIV would be extremely useful.

The second conclusion to be drawn is that blood flow is needed for proper heart development. As demonstrated in the text, in cases where blood flow was obstructed then restarted, the heart exhibited a decrease in contractility, blood velocity, and heart rate, coupled with an increase in edema and regurgitance. Hove *et al.* showed that when blood flow was completely cut off to the heart after 37 hpf, the heart remained in its 37 hpf stage at 4.5 dpf. Our work builds upon these results by showing that even a temporary flow blockage of 8-12 hours

between 48 hpf-72 hpf hinders proper heart development, suggesting that this developmental window is sensitive to flow induced forces.

To better verify the conclusion drawn above, a larger sample size would ideally be collected. More experiments blocking blood flow in fish are needed. While the cases presented here are promising, a larger data set would instill greater confidence in the results. Also, perhaps more importantly, more control cases testing for any effects due to exposure to the magnetic field need to be conducted. The number of controls conducted for the magnetic field was low and plagued by mishaps in the laboratory. To instill more confidence that the effects observed in the fish were solely due to flow blockage, more successful effects from the magnetic field should be ruled out.

The third conclusion to be drawn from this thesis is that the technique described herein is able to deliver and reversibly position small magnetic particles within the vasculature. Utilizing a miniature electromagnet and 250 nm magnetic particles, a bolus of particles was positioned so as to temporarily block blood flow in the tail and to the heart. The ability to introduce the particles at a different location than the heart will allow it to be of use for further heart studies. Perhaps the most important feature of this technique is the reversibility of the flow obstructions. Most flow obstruction techniques have been permanent and invasive. Even with exciting new technologies such as the MicroPoint Nitrogen laser system (Photonics Instruments Inc.), which allows occlusion of specific points within a vessel (Dr. Jay R. Hove, personal communication), one is still faced with a permanent change to the vasculature. With our technique, changes

to the flow can be induced and removed as desired, allowing for more detailed studies in specific developmental windows.

To fully realize the potential of this technique, further research needs to be conducted. For example, the technique needs to be modified to allow for a longer flow alteration time as the maximum flow blockage time in this work was approximately 17 hours. It would be beneficial to be able to keep the blockage in place indefinitely. Additionally, the ability to create specific partial blockages would be useful for further studies linking blood flow with cardiovascular development.

More importantly, the ability to automate the procedure will be vital. As it stands now, this technique can only perform one test case per experiment. In projects where a large sample size is needed, the current technique would prove prohibitively time consuming. An automated array of these magnets would allow many tests per set and increase throughput.

Another area that needs to be addressed is the improvement of the ability to pinpoint the delivery of the magnetic particles. In this work, the particles were delivered to the inflow of the heart. Attempts at positioning the particles inside the heart resulted in the particles being washed downstream. To study problems such as heart valve development it would be desirable to position particles inside the heart, not just at the inflow.

The techniques and results presented in this work may prove useful in a wide range of applications. Beyond the flow studies mentioned above, this technique could possibly be used for targeted drug delivery. With an

improvement in the ability to pinpoint the delivery of magnetic particles, it is conceivable that a similar system could be used in patients to deliver drugs via small magnetic capsules (Lubbe *et al*., 2001; Babincova *et al.,* 2000). For example in the case of an inoperable tumor, a smaller enclosed version of the magnet could be placed, similarly to a wire probe, near the tumor. Drugs could be delivered to the tumor via small magnetic capsules injected into the blood stream that would be attracted by the magnet. A more direct application from our work would be to block blood vessels leading to the tumor. A theoretical technique quite similar to this, but using magnetizable wires, has been proposed by Iacob *et al*. (2004). Computer simulations by Rotariu *et al.* (2004) found that acupuncture needles, magnetized using an external magnetic field, were able to embolize blood vessels leading to tumors using injected micromagnetic particles. The technique developed for the zebrafish flow blockage could be used in the place of magnetized acupuncture needles to provide a more controlled and efficient treatment for patients.

Another potential use of this technique could be in studying flow effects on cultured endothelial cells. One area of current research is the effects of small gradients on adjoining cells (Davies *et al*., 2001) Using a system similar to ours, microscopic obstructions could be placed upstream of individual cells, thereby changing the flow the cell would experience.

The observation that the magnet is able to pull magnetic particles into the tissue is perhaps the most surprising and interesting result. By pulling magnetic particles into selective tissues it may be possible to change the properties of that

tissue. For example, to simulate an infarct, the particles could be drawn into the heart tissue, possibly stiffening it. If so, it seems likely that the contraction in that part of the heart would be reduced, thereby changing cardiac output. This sets the stage for a mechanical means to simulate the effect of infarcts and diseases such as dilated cardiomyopathy in vertebrates. This would serve as an alternative or complementary means of genetic techniques of implementing heart disease, such as experiments by Xu *et al.* (2002), in which alternatively spliced zebrafish genes for *titin* resulted in dilated cardiomyopathy.

A key step in this project, as well as future studies of flow effects on heart development, will be to separate the effects caused by the flow blockage and diminished heart contractility.

Appendix A: Wall Shear Stress Calculations

To ensure that the shear results are not largely dependent on flow profile assumptions, the wall shear stress for a fully developed flow as well as a partially developed flow are presented below.

Shear stress, τ, is defined as the partial derivative of the flow profile.

$\tau = \mu \frac{\partial u(y)}{\partial y}$, where $u(y)$ is the equation for a two dimensional flow profile, with height along the y-axis.

Since the flow from the atrium to the ventricle does not have time to fully develop, a no-slip linear flow profile was assumed. $u(y) = \frac{U}{h} y$, where h is the radius of the vessel. This gives us a shear of

$\tau = \mu \frac{U}{h}$ (1).

For a parabolic flow in a tube of diameter 2h and peak velocity U, the velocity profile is described by the equation:

$u(y) = U[1 - (\frac{y}{h})^2]$.

$\frac{d(u(y))}{dy} = -\frac{2Uy}{h^2}$, to calculate the shear stress at the wall, we set $y = -h$.

Substituting in to $\tau = \mu \frac{\partial u(y)}{\partial y}$ gives us

$\tau = \frac{2\mu U}{h}$ (2),

which is 2 times greater than the shear that would be caused by a linear profile (1).

If one assumes a partially develop flow as modeled below,

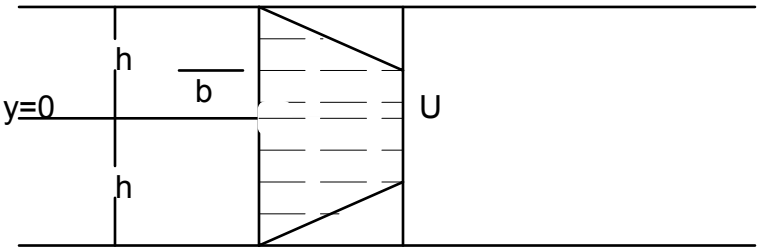

where the velocity profile between $y = b$ and $y = h$ is given by

$$u(y) = \frac{U}{(h-b)} y + b$$

then the shear is described by $\tau = \mu \frac{U}{(h-b)}$ (3),

which is again greater than the shear stress calculated for the linear flow profile (1).

Appendix B: Basic Electromagnetic Theory

Current traveling through a wire gives rise to magnetic field **B** that decays radially away from the wire. A method for calculating the field **B** from a moving current utilized the Biot-Savart Law:

$$\overline{\mathrm{B}} = \frac{\mu_0}{4\pi}\int \frac{id\bar{s}\times\bar{r}}{r^3}$$

where "r" is the radial vector from the current source to the point in space at which the field is being calculated, and "i" is the current.

To find the field in a solenoid, one can get a close approximation by treating the solenoid as a series of individual loops and combine the field created by each one. In the figure below, the solenoid is seen in cross section. At a point "P" inside the solenoid, each of the individual loops contributes to the total magnetic field. Near the center of the solenoid and on the axis, non-axial components of the field cancel out due to symmetry.

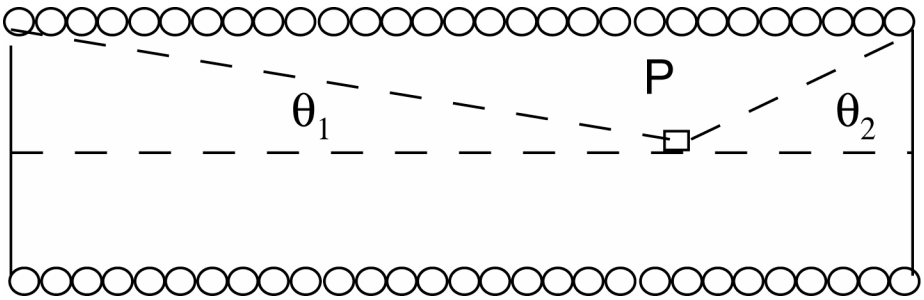

By integrating over the length of the solenoid, one finds that the field in the axial direction along the axis of the solenoid is:

$$B_z = \frac{1}{2}\mu_0 n i_0 (\cos\theta_2 + \cos\theta_1)$$

where n is the number of loops in the solenoid and i_o is the current running through the coil.

In cases of high geometric symmetry Ampere's law can be used to simplify the calculation. Ampere's law states:

$$\oint \overline{\mathrm{B}} \cdot d\overline{s} = \mu_0 \mathrm{I}_{enclosed} .$$

In the case of a solenoid, Ampere's law is quite useful. If one assumes an infinite solenoid, the calculation can be performed as follows:

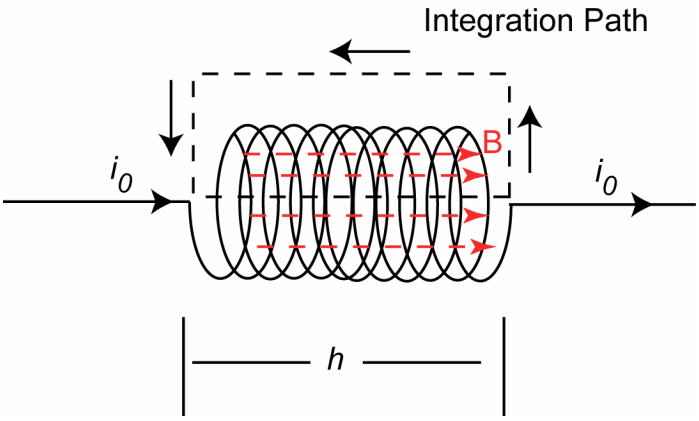

The right hand side of $\oint \overline{\mathrm{B}} \cdot d\overline{s} = \mu_0 \mathrm{I}_{enclosed}$ is non-zero only on the segment of the integration path running through the solenoid and equals **Bh.**

If there are “n” loops per unit length “h” in the solenoid, then the right hand side gives us: $\mu_0 nhi_0$ since $I_{enclosed}$ is equal to i_0 multiplied by number of loops (nh).

This leaves us with $\mathrm{B} = \mu_0 n i_0$. If one takes the result of the finite solenoid and takes the limit as the length goes to infinity, both angles go to zero, and the result becomes

$\mathrm{B} = \mu_0 n i_0$.

It should be noted that this result is for an ideal solenoid in which the length is much greater than its diameter. Barbic’s magnet has a length that is not that much greater than the radius. As such, to be precise, edge effects would have to be taken into account. However, for the most part, we can assume a constant field in the interior of the coil.

In the magnet used in these experiments, the coils of the solenoid were wrapped around a ferromagnetic core, which increases the total magnetic field emanating from the solenoid.

In this case the core gets magnetized and obtains a magnetization that is defined as the net dipole moment per unit volume,

$\overline{M} = \frac{\sum \overline{\mu}_i}{V}$, where μ is a dipole moment and V is the volume.

When the material is placed in the solenoid's magnetic field, all of the dipoles in the material align in the direction of the field and create their own magnetic field in the same direction.

Therefore the total magnetic field is a combination of B_0, the field from the solenoid, and the field produced by the aligned dipole, $B_m = \mu_0 \mathbf{M}$. The magnetic field from the core is generally much greater than the field from the solenoid; however, it is not easy to measure or determine the field strength directly in our device.

Force experienced by a particle due to this electromagnet.

The force on the bead from the magnet is a result of the field strength as well as the magnetic field gradient at the bead.

$$\mathbf{F}_{\mathbf{bead}} = (\mathbf{m}_{\mathbf{bead}}(\mathbf{B}_{\mathbf{total}}) \cdot \nabla)\mathbf{B}_{\mathbf{total}}$$

The small size and sharp tip of the electromagnet work to enhance the field and field gradient produced, and therefore maximize the magnetic force on the sample being manipulated.

References

Babincova, M., Altanerova, V., Lambert, M., Altaner, C., Sramka, M., Machova, E. and Babinec, P. 2000. Site specific in vivo targeting of magnetolipozomes in external magnetic field. *Z. Naturforsch* **55c:** 278-282

Barbic, M., Mock, J.J., Gray, A.P. and Schultz S. 2001. Scanning probe electromagnetic tweezers. *Applied Physics Letters* **79(12):** 1897-1899

Bartmann, T., Walsh, E.C., Wen., K., McKane, M., Ren, J., Alexander, J., Rubenstein, P.A. and Stanier, D.Y.R. 2004. Early myocardial function affects endocardial cushion development in zebrafish. *PLOS Biology* **2(5):** 673-681

Bremer, J.L. 1932. The presence and influence of two spiral streams in the heart of the chick embryo. *American Journal of Anatomy* **49:** 409-440

Bruneau, B.G. 2002. Transcriptional regulation of vertebrate cardiac morphogenesis. *Circulation Research* **90:** 509-519

Caro, C.G., Fitz-Gerald, J.M. and Schroter, R.C. 1969. Atheroma and arterial wall shear: observation, correlation and proposal of a shear dependent mass transfer mechanism for atherogenesis. *Proceedings Royal Society London* **177:** 109-159

Chen, J.N., van Eeden, F.J.M., Warren, K.S., Chin, A., Nusslein-Volhard, C., Haffter, P. and Fishman, M.C. 1997. Left-right pattern of cardiac BMP4 may drive asymmetry of the heart in zebrafish. *Development* **124:** 4373-4382

Chin, A.J., Tsang, M. and Weinberg, E.S. 2000. Heart and gut chiralities are controlled independently from initial heart position in developing zebrafish. *Developmental Biology* **227(2):** 403-421

Clark, E.B. and Hu, N. 1982. Developmental hemodynamics changes in the chick embryo from stage 18 to 27. *Circulation Research* **51(6):** 810-815

Clark, E.B., Hu, N. and Rosenquist, G.C. 1984. Effect of conotruncal constriction on aortic mitral-valve continuity in the stage-18, stage-21 and stage-24 chick-embryo. *American Journal of Cardiology* **53(2):** 324-327

Coates, C.G., Denvir, D.J., McHale, N.G., Thornbury, K.D. and Hollywood, M.A. 2004. Optimizing low-light microscopy with back-illuminated electron multiplying charge-coupled device. *Journal of Biomedical Optics* **9(6):** 1244-1252

Creazzo, T.L., Godt, R.E., Leatherury, L., Conway, S.J. and Kirby, M.L. 1998. Role of cardiac neural crest cells in cardiovascular development. *Ann. Rev. Physiology* **60:** 267-86

Davies, P.F. 1989. How do vascular endothelial cells respond to flow? *News in Physiological Sciences* **4:** 22-25

Davies, P.F., Mundel, T. and Barbee, K.A. 1995. A mechanism for heterogeneous endothelial responses to flow in vivo and in vitro. *Journal of Biomechanics* **28:** 1553-60.

Davies, P.F., Shi, C., Depaola, N., Helmke, B.P. and Polacek, D.C. 2001. Hemodynamics and the focal origin of atherosclerosis: a spatial approach to endothelial structure, gene expression, and function. *Annals of the New York Academy of Sciences* **947:** 7-16; discussion 16-7

DeBakey M.E, Gotto Jr., A.M. 1997. The new living heart. Adams Media Corporation p. 325

Devansenathipahty, S., Santiago, J.G., Wereley, S.T., Meinhart, C.D. and Takehara, K. 2003. Particle imaging techniques for microfabricated fluidic systems. *Experiments in Fluids* **34:** 504-514

Dewey Jr., C.F. Bussolari, S.R., Gimbrone Jr., M.A. and Davies, P.F. 1981. The dynamic response of vascular endothelial cells to fluid shear stress. *Journal of Biomechanical Engineering* **103:** 177-185

Eisenberg, L.M. and Markwald, R.R. 1995. Molecular regulation of atrioventricular valvuloseptal morphogenesis. *Circulation Research* **77(1)** 1-6

Ekman, G. 1925. Experimentelle Beitrage zur Herzentwicklung der Amphibien. *Roux. Arch. Entwickl. –Mech. Org.* **106:** 320

Fishman, M.C. and Chien, K.R. 1997. Fashioning the verebrate heart: earliest embryonic decisions*. Development* **124:** 2099-2117

Fox J.A. and Hugh A.E. 1966. Localization of atheroma: a theory based on boundary layer separation. *British Heart Journal*. **26:** 388-399

Fry D.L. 1968. Acute vascular endothelial changes associated with increased blood velocity gradients. *Circulation Research* **22:** 165-197

Gharib M. and Beizaie M. 2003. Correlation between negative near-wall shear stress in human aorta and various stages of congestive heart failure. *Annals of Biomedical Engineering* **31 (6)**: 678-685

Gharib, M. and Dabiri, D. 2000. “An overview of digital particle image velocimetry” in *Flow Visualization: Techniques and Examples*, Eds. Smits, A. and Lim, T.T. London, Imperial College Press, March

Haugton, V.M., Korosec, F.R., Medow, J.E., Dolar, M.T. and Iskandar, B.J. 2003. Peak systolic and diastolic csf velocity in the foramen magnum in adult patients with chiari I malformations and in normal control participants. *American Journal of Neuroradiology* **24:** 169-176

Hayes, M.A., Polson, N.A. and Garcia, A.A. 2001. Active control of dynamic supraparticle structures in microchannels*. Langmuir* **17(9):** 2866-2871

Hogers, B., DeRuiter, M.C., GittenbergerdeGroot, A.C. and Poelmam, R.E. 1997. Unilateral vitelline vein ligation alters intracardiac blood flow patterns and morphogenesis in the chick embryo. *Circulation Research* **80 (4):** 473-481

Hove, J.R. 2004. In vivo biofluid dynamic imaging in the developing zebrafish. *Birth Defects Research (Part C)* **72:** 277-289

Hove, J.R., Köster, R., Forouhar, A.S., Acevedo-Bolton, G., Fraser, S.E. and Gharib, M. 2003. Intracardiac fluid forces are an essential epigenetic factor for embryonic cardiogenesis. *Nature* **421:** 172-177

Hu N., Sedmera, D., Yost, H.J. and Clark, E.B. 2000. Structure and function of the developing zebrafish heart**.** *The Anatomical Record* **260:** 148-157

Hu, N., Yost, H.J. and Clark, E.B. 2001. Cardiac morphology and blood pressure in the adult zebrafish. *The Anatomical Record* **264:** 1-12

Iacob, G., Rotariu, O., Strachan, N.J. and Hafeli, U.O. 2004. Magnetizable needles and wires—Modeling an efficient way to target magnetic microspheres in vivo. *Biorheology* **41(5):** 599-612

Jones E.A.V., Baron, M.H., Fraser, S.E. and Dickinson, M.E. 2004. Measuring hemodynamic changes during mammalian development. *American Journal of Physiology-Heart and Circulatory Physiology* **287:** H1561-H1569

Jou, L.D. and Berger, S.A. 1998. Numerical Simulation of the flow in the Carotid Bifurcation*. Theoretical Computational Fluid Dynamics* **10**: 239-248

Jou, L.D. and Saloner, D. 1998 A numerical study of magnetic resonance images of pulsatile flow in a two dimensional carotid bifurcation—A numerical study of MR images. *Medical Engineering Physics* **20(9):** 643-652

Karlsson, J., von Hofsten J. and Olsson, P.E. 2001. Generating transparent zebrafish: a refined method to improve detection of gene expression during embryonic development. *Marine Biotechnology(NY)* **3:** 522-527

Kilner, P.J., Yang, G.Z. and Firmin, D.N. 2002. Morphodynamics of flow through sinuous curvatures of the heart. *Biorheology* **39(3-4):** 409-17

Kimmel, C.B., Ballard, W.W., Kimmel, S.R., Ullmann, B. and Schilling, T.F. 1995. Stages of embryonic Development of the Zebrafish. *Developmental Dynamics* **203:** 253-310

Koutsiaris, A.G. and Pogiatzi A. 2003. Velocity pulse measurements in the mesenteric arterioles of rabbits. *Physiological Measurement* **25:** 15-25

Long, Q., Meng, A., Wang, H., Jessen, J.R., Farrell, M.J. and Lin, S. 1997. GATA-1 expression pattern can be recapitulated in living transgenic zebrafish using GFP reporter gene. *Development* **124:** 4105-4111

Lubbe, A.S., Alexiou, C. and Bergemann, C. 2001. Clinical applications of magnetic drug targeting. *Journal of Surgical Research* **95:** 200-206

Malek, A.M., Alper, S.L. and Izumo, S. 1999. Hemodynamic shear stress and its role in atherosclerosis. *JAMA* **282(21):** 2035-2042

Manasek, F.J. and Monroe, R.G. 1972, Early cardiac morphogenesis is independent of function. *Developmental Biology* **27:** 584-588.

Meinhart, C.D., Wereley, S.T. and Santiago, J.G. 1999. PIV measurements of a microchannel flow. *Experiments in Fluids* **27:** 414-419

Nakano, A., 2002. Spinning-disk confocal microscopy–A cutting edge tool for imaging of membrane traffic. *Cell Structure and Function* **27:** 349-355

Nakano A., Sugii, Y., Minamiyama, M. and Niimi, H. 2003. Measurement of red blood cell velocity in microvessels using particle image velocimetry (PIV). *Clinical Hemorhealogy and Microcirculation* **29:** 445-455

Nerem, R.M., Harrison, D.G., Taylor, W.R. and Alexander, R.W. 1993. Hemodynamics and vascular endothelial biology. *Journal of Cardiovascular Pharmacology* **21**: S6-S10 Suppl. 1

O'Brien, S.P.M., Wheeler, T., and Barker, D.J.P. 1999. Fetal programming influences on development and disease later in life. RCOG, London

Olesen, S.P., Clapham, D.E. and Davies, P.F. 1988. Hemodynamic stress-activates a K^+ current in vascular endothelial-cell morphology. *Nature* **331:** 168-170

Olson, E.N. and Srivastava, D. 1996. Molecular pathways controlling heart development. *Science* **272:** 671-676

Pelster, B. and Burggren, W.W. 1996. Disruption of hemoglobin oxygen transport does not impact oxygen-dependent physiological processes in developing embryos of zebra fish (*Danio rerio)*. *Circulation Research* **79:** *358-362*

Phoon, C.K. and Turnbull, D.H. 2003. Ultrasound biomicroscopy-Doppler in mouse cardiovascular development. *Physiological Genomics* **14:** 3-15

Reiter, J.F., Alexander, J., Rodaway, A., Yelon, D., Patient, R., Holder, N. and Stainer, D.Y. 1999. Gata5 is required for the development of the heart and endoderm in zebrafish. *Genes Dev.* **13:** 2983-2995

Rotariu, O., Iacob, G., Strachan, N.J.C. and Chiriac, H. 2004. Simulating the embolization of blood vessels using magnetic microparticles and acupuncture needle in a magnetic field. *Biotechnology Progress* **20:** 299-305

Roux, W. 1895. Gesammelte Abhandlungen uber Entwickelungsmechanik der Organismen. 2 vol. Englemann, Leipzig

Sedmera, D., Pexieder, T., Rychterova, V., Hu, N. and Clark E.B. 1999. Remodeling of chick embryonic ventricular myoarchitecture under experimentally changed loading conditions. *Anatomical Record* **254(2):** 238-252

Sehnert, A.J., Huq, A., Weinstein, B.M., Walker, C. and Fishman, M.C. 2002. Cardiac troponin T is essential in sarcomere assembly and cardiac contractility. *Nature Genetics* **31:** 106-110

Schwerte, T. and Pelster, B. 2000. Digital motion analysis as a tool for analyzing the shape and performance of the circulatory system in transparent animals. *Journal of Experimental Biology* **203:** 1659-1669

Stanier, D.Y.R. 2001. Zebrafish genetics and vertebrate heart formation. *Nature Reviews* **2:** 39-48

Stanier, D.Y.R., Fouquet, B., Chen, J., Warren, K.S., Weinstein, B.M., Meiler, S.E., Mohideen, M.P.K., Neuhauss, S.C.F., Solnica-Krezel, L., Schier, A.F., Zwartkruis, F., Stemple, D.L., Malicki, J., Driever, W. and Fishman, M.C. 1996. Mutations affecting the formation and function of the cardiovascular system in the zebrafish embryo. *Development* **123:** 285-292

Stanier, D.Y.R., Lee, R.K. and Fishman, M.C. 1993. Cardiovascular development in the zebrafish. Myocardial fate map and heart tube formation. *Development* **119:**31-40

Stohr, P. Jr. 1924. Experimentelle Studien an embryonalen Amphibienherzen. I. Uber Explanation Embryonaler Amphibienherzen. *Roux Arch. Entwickl. Mech. Org.* **102:** 426-451

Stohr, P. Jr. 1925. Experimentelle Studien an embryonalen Amphibienherzen. III. Uber die Entstehung der Herzform. *Roux Arch. Entwickl. Mech. Org.* **106:** 409-455

Stohr, P. Jr. 1927. Experimentelle Studien an embryonalen Amphibienherzen. IV. *Roux Arch. Entwickl. Mech. Org.* **112:** 696-738

Streisinger, G., Walker, C., Dower, N., Knauber, D. and Singer, F. 1981. Production of clones of homozygous diploid fish (*Brachydanio rerio*). *Nature* **291:** 293-296

Sugii, Y., Nishio, S. and Okamoto, K. 2002. *In vivo* PIV measurement of red blood cell velocity in microvessels considering mesentery motion. *Physiological Measurement* **23:** 403-416

Taber, L.A. 1998. Mechanical aspects of cardiac development. *Prog. Biophys. Mol. Biol.* **69:** 237-255

Takahashi, M., Ishida, T., Traub, O., Corson, M.A. and Berk, B.C. 1997. Mechanotransduction in endothelial cells: Temporal signaling events in response to shear stress. *Journal of Vascular Research* **34:** 212-219

Takehara, K., Adrian, R.J., Etoh, G.T. and Christensen, K.T. 2000. A Kalman tracker for super-resolution PIV. *Experiments in Fluids* **29:** S34-S41

Thisse, C. and Zon, L.I. 2002. Organogenesis-heart and blood formation from the zebrafish point of view. *Science* **295:** 457-462

Tsuchiya, K., Aoki, C., Fujikawa, A. and Hachiya, J. 2004 Three-dimensional MR digital subtraction angiography using parallel imaging and keyhole data sampling in cerebrovascular disease: initial experience. *European Radiology* **14(8):** 1494-1497

Warren, K.S. and Fishman, M.C. 1998. "Physiological genomics": mutant screens in zebrafish. *American Journal of Physiology-Heart and Circulatory Physiology* **275 (1):** H1-H7

Weinstein, B.M. 2002. Vascular cell biology in vivo: a new piscine paradigm? *Trends in Cell Biology* **12:** 439-445

Weinstein, B.M., Stemple, D.L., Driever, W. and Fishman, M.C. 1995. Gridlock, alocalized heritable vascular patterning defect in the zebrafish. *Nature Medicine* **1:** 1143-1147

Westerfield, M. 2000. The zebrafish book. A guide for the laboratory use of zebrafish (*Danio rerio)*. 4th ed. Eugene, Or: University of Oregon Press.

Westerweel, J. 1993. Digital particle image velocimetry -Theory and application. University Press (Delft): Ph.D. thesis

Willert,C.E. 1992. The interaction of modulated vortex pairs with a free surface. University of California, San Diego: Ph.D. thesis

Willert, C.E. and Gharib, M. 1991. Digital particle image velocimetry. *Experiments in Fluids* **10:** 181-193

Yelon, D., Horne, S.A. and Stanier D.Y. 1999. Restricted expression of cardiac myosin genes reveals regulated aspects of heart tube assembly in zebrafish. *Developmental Biology* **214(1):** 23-37

Yelon, D., Ticho, B., Halpern, M.E., Ruvinsky, I., Ho, R.K., Silver, L.M. and Stanier, D.Y. 2000. The bHLH transcription factor hand2 plays parallel roles in zebrafish heart and pectoral fin development. *Development* **127:** 2573-2582

Yoshida, H., Manasek, F. and Arcilla, R.A. 1983. Intracardiac flow patterns in early embryonic life a reexamination. *Circulation Research* **53(3):** 363-371

Xu, X., Meiler, S.E., Zhong, T.P., Mohideen, M., Crossley, D.A., Burggren, W.W. and Fishman, M.C. 2002. Cardiomyopathy in zebrafish due to mutation in an alternatively spliced exon of *titin. Nature Genetics* **30:** 205-209